Atmos. Chem. Phys. Discuss., 11, 15497–15550, 2011
www.atmos-chem-phys-discuss.net/11/15497/2011/
doi:10.5194/acpd-11-15497-2011

Atmospheric Chemistry and Physics Discussions

A comprehensive numerical study of aerosol-cloud-precipitation interactions in marine stratocumulus

Y.-C. Chen[1], L. Xue[2], Z. J. Lebo[1], H. Wang[3], R. M. Rasmussen[2], and J. H. Seinfeld[1,4]

[1]Division of Engineering and Applied Science, California Institute of Technology, Pasadena, California, USA
[2]National Center for Atmospheric Research (NCAR), Boulder, Colorado, USA
[3]Pacific Northwest National Laboratory (PNNL), Richland, Washington, USA
[4]Division of Chemistry and Chemical Engineering, California Institute of Technology, Pasadena, California, USA

Received: 13 May 2011 – Accepted: 13 May 2011 – Published: 20 May 2011

Correspondence to: J. H. Seinfeld (seinfeld@caltech.edu)

Published by Copernicus Publications on behalf of the European Geosciences Union.

Abstract

Three-dimensional large-eddy simulations (LES) with detailed bin-resolved microphysics are performed to explore the diurnal variation of marine stratocumulus (MSc) clouds under clean and polluted conditions. The sensitivity of the aerosol-cloud-precipitation interactions to variation of sea surface temperature, free tropospheric humidity, large-scale divergence rate, and wind speed is assessed. The comprehensive set of simulations corroborates previous studies that (1) with moderate/heavy drizzle, an increase in aerosol leads to an increase in cloud thickness; and (2) with non/light drizzle, an increase in aerosol results in a thinner cloud, due to the pronounced effect on entrainment. It is shown that for higher SST, stronger large-scale divergence, drier free troposphere, or lower wind speed, the cloud thins and precipitation decreases. The sign and magnitude of the Twomey effect, droplet dispersion effect, cloud thickness effect, and overall cloud optical depth susceptibility to aerosol perturbations are evaluated by LES experiments and compared with analytical formulations. The Twomey effect emerges as dominant in total cloud susceptibility to aerosol perturbations. The dispersion effect, that of aerosol perturbations on the cloud droplet size spectrum, is positive (i.e., increase in aerosol leads to spectral narrowing) and accounts for 3 % to 10 % of the total cloud susceptibility at nighttime, with the largest influence in heavier drizzling clouds. The cloud thickness effect is negative (i.e., increase in aerosol leads to thinner cloud) for non/light drizzling cloud and positive for moderate/heavy drizzling clouds; the cloud thickness effect contributes 5 % to 22 % of the nighttime cloud susceptibility. The range of magnitude for each effect is more variable in the daytime owing to cloud thinning and decoupling. Overall, the cloud susceptibility is ~0.28 to 0.53 at night; an increase in aerosol concentration enhances cloud optical depth, especially with heavier precipitation and in a more pristine environment. The good agreement between LES experiments and analytical formulations suggests that the latter may be useful in evaluations of cloud susceptibility. The ratio of the magnitude of the cloud thickness effect to that of the Twomey effect depends on cloud base height and cloud

thickness in unperturbed (clean) clouds.

1 Introduction

Aerosols influence the microphysical properties of clouds and hence affect their radiative properties, amount, and lifetime (IPCC, 2007). This influence, termed the aerosol indirect effect on climate, is identified as one of the major uncertainties in a quantitative assessment of the anthropogenic radiative forcing of climate. Marine stratocumulus clouds (MSc) play a significant role in the Earth's radiation budget. Covering about one-third of the world's oceans (Warren et al., 1988), MSc are particularly susceptible to the effect of aerosol perturbations. These clouds are generally optically thick and exist at a low altitude, making them more effective at reflecting solar radiation (albedo is about 30–40 %, Randall et al., 1984) than at trapping terrestrial radiation. It has been estimated that a 6 % increase of the albedo in MSc regions (equivalent to about a $0.2\,\mathrm{g\,kg^{-1}}$ moistening of the marine boundary layer (MBL), or an increase in cloud droplet number concentration N_d from 75 to $150\,\mathrm{cm^{-3}}$) could result in a $1\,\mathrm{W\,m^{-2}}$ change in the net solar radiation at the top of the atmosphere (Stevens and Brenguier, 2009).

The complex interactions of the cloud system involve aerosol and cloud microphysics, atmospheric dynamics, radiation, and chemistry (See, for example, Stevens and Feingold, 2009). Representations of the dynamic and thermodynamic state of MSc have been the subject of several reviews (e.g., Stevens, 2005, 2006) and numerous modeling studies. Mixed-layer models (MLMs, Lilly, 1968) couple cloud, radiation, and turbulence to describe the cloud-topped MBL (e.g., Turton and Nicholls, 1987; Bretherton and Wyant, 1997; Lilly, 2002; Wood, 2007; Sandu et al., 2009; Caldwell and Bretherton, 2009a; Uchida et al., 2010). Given surface and free-tropospheric thermodynamic conditions, bulk cloud properties, such as thickness, cloud liquid water path (LWP), and the MBL steady-state, can be determined by an MLM. The MLM framework represents a well-mixed MBL. Departures from well-mixed conditions are, however, common in situations of precipitation and during daytime.

Discussion Paper | Discussion Paper | Discussion Paper | Discussion Paper |
ACPD
11, 15497–15550, 2011
Aerosol-cloud-precipitation interactions in MSc
Y.-C. Chen et al.

To represent both MSc microphysics and dynamics, large-eddy simulations (LES) have become a powerful tool because of the ability to realistically represent the larger eddy turbulence field and the interactions of turbulence, cloud microphysics and radiation at an appropriate grid resolution. LES has been applied in many previous studies of MSc (e.g., Stevens et al., 1998, 2003, 2005; Stevens and Bretherton, 1999; Bretherton et al., 1999; Chlond and Wolkau, 2000; Jiang et al., 2002; Wang et al., 2003; Duynkerke et al., 2004; Lu and Seinfeld, 2005, 2006; Bretherton et al., 2007; Sandu et al., 2008; Savic-Jovcic and Stevens, 2008; Yamaguchi and Randall, 2008; Hill et al., 2008, 2009; Ackerman et al., 2009; Caldwell and Bretherton, 2009b; Wang and Feingold, 2009a,b; Wang et al., 2010; Uchida et al., 2010). Table 1 summarizes a number of studies that focus mainly on aerosol-cloud interactions in MSc; these address the LWP responses to changes in aerosol number and ambient environmental conditions, including sea surface temperature (SST), large scale divergence rate (D), and free tropospheric humidity (q_{ft}). Atmospheric aerosols and meteorology each exert controls on cloudiness; the former governs the cloud micro-structure, while the latter provides the dynamic and thermodynamic state that controls cloud macro-structure (Stevens and Brenguier, 2009).

A number of effects of aerosol perturbations on cloud LWP, cloud lifetime, and precipitation have been predicted by numerical studies and, in some cases, identified by measurements. Overall, the causality that has been proposed for aerosol-cloud-precipitation interactions can be summarized as follows:

(a) Twomey effect (assumes constant LWP): aerosol number concentration (N_{a}) increase → smaller, more numerous droplets → higher albedo (Twomey, 1977)

(b) Albrecht effect (drizzling cloud): N_{a} increase → smaller, more numerous droplets → reduced collision-coalescence → less precipitation → LWP increase → higher albedo (Albrecht, 1989)

(c) Drizzle-entrainment effect (drizzling cloud): N_{a} increase → smaller, more numerous droplets → reduced collision-coalescence → less precipitation → reduced

ACPD
11, 15497–15550, 2011
Aerosol-cloud-precipitation interactions in MSc
Y.-C. Chen et al.

below-cloud evaporative cooling and in-cloud latent heat release → higher turbulent kinetic energy (TKE) → stronger entrainment → LWP decrease → lower albedo (e.g., Lu and Seinfeld, 2005; Wood, 2007)

(d) Sedimentation-entrainment effect (non-drizzling cloud): N_a increase → smaller, more numerous droplets → reduced in-cloud sedimentation → increase of cloud water and evaporation in entrainment regions → stronger entrainment → LWP decrease → lower albedo (Ackerman et al., 2004; Bretherton et al., 2007; Hill et al., 2009)

(e) Evaporation-entrainment effect (non-drizzling cloud): N_a increase → smaller, more numerous droplets → more efficient evaporation → higher TKE → stronger entrainment → LWP decrease → lower albedo (Wang et al., 2003; Xue and Feingold, 2006; Hill et al., 2008)

Drizzle formation leads to release of latent heat in the cloud and to stabilization of the sub-cloud layer through evaporative cooling and moistening. Thus the existence of drizzle reduces the buoyancy, stabilizes the MBL, decreases the TKE, and reduces the entrainment strength. As a result, precipitation suppression due to increased N_a increases the buoyancy fluxes and TKE, destabilizes the MBL, and enhances the cloud-top entrainment (as shown in pathway (c)) (e.g., Stevens et al., 1998; Ackerman et al., 2004; Lu and Seinfeld, 2005; Wood, 2007).

Aerosol-cloud interactions in non-drizzling MSc can be influenced by two kinds of entrainment effects (Hill et al., 2009): (d) Sedimentation-entrainment effect: increasing N_a in nondrizzling MSc reduces in-cloud sedimentation, and thus increases the cloud liquid water content and evaporation in the entrainment region, leading to stronger entrainment and LWP reduction (Bretherton et al., 2007); (e) Evaporation-entrainment effect: increase in N_a results in smaller, more numerous cloud droplets, and thus stronger evaporation, which enhances in-cloud turbulence and cloud-top entrainment. The entrained warm, dry air leads to cloud thinning and LWP reduction (Wang et al., 2003;

Xue and Feingold, 2006). For both effects an increase in N_a leads to LWP reduction, counteracting (b).

In simulations of MSc, Ackerman et al. (2004) showed that when surface precipitation rate exceeds ~0.1 mm day^{-1}, the LWP increases with N_d (following effect (b)). Similar trends have also been found in other nocturnal studies (Table 1), in which opposite responses of LWP to an increase in N_a for moderate/heavy and non/light drizzling conditions occur. The free troposphere moisture (q_{ft}) exerts a strong control on the precipitation rate through cloud-top entrainment, thus altering the balance between the competing effects of precipitation on LWP. The effects of the free tropospheric moisture can be summarized (Ackerman et al., 2004) as: (1) moist entrained air → does not dry MBL effectively → cloud thickening, versus (2) dry entrained air → dry the MBL → cloud thinning. Similar results were also obtained by Sandu et al. (2008) for a diurnal cycle.

The effect of changes in the large scale divergence, *D*, is consistent among the studies listed in Table 1, showing that under higher (lower) *D*, the cloud top is driven down deeper (shallower), resulting in thinner (thicker) cloud, lower (higher) LWP. Since *D* is difficult to measure, its value is usually estimated.

The effect of changes in SST on MSc has been addressed in several studies. In the LES study of Lu and Seinfeld (2005), the initial temperature in the entire MBL was assumed to increase systematically with SST, and the MBL relative humidity was adjusted as well. It is found that with higher SST, the MBL deepens and cloud base rises, resulting in a thinner cloud with lower LWP. And the MSc becomes less cloudy because of gradual dissipation. In the MLM study of Caldwell and Bretherton (2009a), however, as SST increases, the equilibrium cloud base and cloud top heights both increase due to increased entrainment through a weaker inversion, resulting in a thicker cloud with higher LWP. Therefore in response to a higher SST, shorter time scale and equilibrium responses have different effects on MSc.

Diurnal variation is the result of competition between cloud top longwave (LW) radiative cooling occurring both day and night, and daytime solar heating (Hill et al., 2008).

ACPD
11, 15497–15550, 2011

During nighttime, cloud top LW cooling enhances TKE, couples the cloud and the surface fluxes, well mixes the MBL, and the cloud tends to become thicker. While under daytime conditions, absorption of solar radiation offsets the cloud top LW cooling, stabilizing the MBL, causing the cloud to thin; some clouds may even become decoupled. Predicted daytime LWP is consistently smaller than that in nighttime (Table 1). Also, daytime MBL is less sensitive to changing N_a than under nighttime conditions (e.g., Ackerman et al., 2004; Lu and Seinfeld, 2005), suggesting cloud-radiation interactions are important in controlling the diurnal variation.

From a summary of the studies cited in Table 1, overall, non/light drizzling MSc and moderate/heavy drizzling MSc respond differently to changes in aerosol level since the dominant physical/dynamical mechanisms differ. Also, distinct diurnal responses are shown in day and nighttime conditions as a result of cloud-radiation interactions. And MSc is found to be sensitive to changes in ambient conditions, e.g., SST, D, or q_{ft}.

Aerosol-cloud-precipitation interactions in MSc are tightly intertwined and often subtle. In order to obtain a comprehensive view of these interactions, high-resolution LES simulations are carried out in the present study. The meteorological factors investigated include SST, free-tropospheric humidity, large scale subsidence rate, and wind speed. Diurnal variation is considered as well as non/light drizzling and moderate/heavy drizzling MSc. We begin with an analytical formulation of cloud susceptibility to aerosol perturbation in terms of the Twomey, droplet dispersion, cloud thickness, and diabaticity effects. The sign and magnitude of each effect are evaluated from LES experiments to compare with the analytical formulations. While each of the studies cited in Table 1 addresses one or more aspects of aerosol-MSc interactions, the present study is intended to be a comprehensive, consistent evaluation of these interactions covering the range of the important variables.

Discussion Paper | Discussion Paper | Discussion Paper | Discussion Paper |

ACPD

11, 15497–15550, 2011

2 Cloud susceptibility to aerosol perturbations

Before proceeding to the numerical study, it is useful to address MSc aerosol-cloud relationship from a simplified analytical point of view, providing a consistent basis on which to connect aerosol-cloud-precipitation interactions. Considering the change of cloud radiative properties in response to a change in aerosol number concentration, N_a, the relationship between adiabatic cloud optical thickness ad and adiabatic cloud droplet number concentration, N_{ad}, can be expressed (Brenguier et al., 2000):

$$\tau_{ad} = \frac{9}{10}\left(\frac{4}{3}\pi\right)^{\frac{1}{3}} l_o^{\frac{2}{3}} (kN_{ad})^{\frac{1}{3}} H^{\frac{5}{3}}, \tag{1}$$

where $l_0 = C_w/\rho_w$, ρ_w is the density of water, C_w is the moist adiabatic condensation coefficient, k is a parameter related to the droplet spectrum shape, which is inversely proportional to the droplet distribution breadth, and H is cloud thickness. The range of k is 1 in the limit of a monodisperse size distribution and approaches 0 for a very wide distribution. In the presence of cloud top entrainment and water loss through precipitation, the cloud droplet profile tends to be diabatic. A sub-adiabaticity parameter f can be defined to include the effects of entrainment and precipitation in drying out the cloud relative to the adiabatic case. Equation (1) can be generalized (W. Conant, unpublished, 2005) as

$$\tau = \frac{9}{10}\left(\frac{4}{3}\pi\right)^{\frac{1}{3}} l_o^{\frac{2}{3}} (1-f)^{\frac{(2+m)}{3}} (kN_{ad})^{\frac{1}{3}} H^{\frac{5}{3}}, \tag{2}$$

where f is 0 under adiabatic conditions, and approaches 1 under cloud-free conditions. The parameter m describes the microphysical impacts of mixing between the cloudy air and the relatively dry/warm free tropospheric air. $m = 1$ corresponds to the limit of inhomogeneous mixing, in which the turbulent mixing is relatively slow and all droplets in the entrained air evaporate, resulting in reduction of N_d and broadening of the droplet spectrum. $m = 0$ corresponds to the limit of homogeneous mixing, in which the timescale of turbulent mixing is much shorter than that at which droplets respond to the fresh ambient air. In this limit, all droplets experience the same degree of subsaturation and evaporate together; thus N_d remains constant as all droplets shift to smaller sizes.

From Eq. (2), the impact of changes in aerosol number concentration on cloud optical depth (the cloud susceptibility) can be expressed as follows:

$$\frac{d\ln\tau}{d\ln N_\mathrm{a}} = \frac{1}{3}\left(\frac{d\ln N_\mathrm{ad}}{d\ln N_\mathrm{a}} + \frac{d\ln k}{d\ln N_\mathrm{a}} + 5\frac{d\ln H}{d\ln N_\mathrm{a}} - (2+m)\frac{d\ln f}{d\ln N_\mathrm{a}}\right). \tag{3}$$

2.1 Twomey effect

From the above equation, $d\ln N_\mathrm{ad}/d\ln N_\mathrm{a}$ represents the so-called Twomey effect. An analytical relationship between N_ad and N_a, modified from that derived by Twomey (1959), is

$$N_\mathrm{ad} = N_\mathrm{a}^{\frac{2}{k_\mathrm{s}+2}}\left(\frac{cw^{\frac{3}{2}}}{k_\mathrm{s}B\left(\frac{k_\mathrm{s}}{2},\frac{3}{2}\right)}\right)^{k_\mathrm{s}/(k_\mathrm{s}+2)}, \tag{4}$$

where B is the beta function, w is updraft velocity at cloud base, k_s is a parameter related to the exponent in an assumed power-law aerosol size distribution, and c is a composition-dependent parameter that relates the aerosol size distribution to the supersaturation spectrum. From Eq. (4),

$$\frac{d\ln N_\mathrm{ad}}{d\ln N_\mathrm{a}} = \frac{2}{k_\mathrm{s}+2}. \tag{5}$$

Values of k_s range from 0.3 to 1.4 (empirical constants for cloud condensation nuclei, CCN, at 1 % supersaturation, from Pruppacher and Klett, 1997). For that range, $d\ln N_\mathrm{ad}/d\ln N_\mathrm{a}$ varies from about 0.6–0.9 under adiabatic conditions. Shao and Liu

ACPD
11, 15497–15550, 2011

Aerosol-cloud-precipitation interactions in MSc

Y.-C. Chen et al.

(2009) compared $d\ln N_{ad}/d\ln N_a$ predicted by Eq. (5) with in-situ measurements (values of 0.25–0.85). Differences in the value of $d\ln N_{ad}/d\ln N_a$ between the analytical expression and ambient measurements can be attributed to (1) activation effect: adding aerosols, for example, into a marine aerosol background reduces the ability of aerosols to act as CCN, and (2) adiabaticity influence: the variability of the adiabaticity (cloud dilution state) from different meteorological conditions between clean and polluted clouds.

2.2 Dispersion effect

The second term $d\ln k/d\ln N_a$ expresses the effect of changes in N_a on the cloud droplet size distribution. Dispersion in the droplet distribution is related to aerosol composition (e.g., Feingold and Chuang, 2002), microphysics (e.g., collision-coalescence), and dynamics (e.g., entrainment mixing, updraft velocity) (Wood et al., 2002; Lu and Seinfeld, 2006). It is noted from observational data (Martin et al., 1994; Ackerman et al., 2000; Liu and Daum, 2002) that the dispersion forcing would lead to an indirect warming effect, opposing the Twomey effect. Accounting for the parameterization of dispersion effect in GCMs leads to a reduction in the magnitude of the predicted Twomey effect (Rotstayn and Liu, 2003, 2009). By contrast, an opposite trend is found in the LES study of Lu and Seinfeld (2006). For a drizzling cloud, increasing N_a leads to spectrum narrowing (larger k) because smaller droplets suppress precipitation formation by limiting the collision-coalescence process and enhance droplet condensational growth in the presence of higher updraft velocities, due to stronger TKE (Lu and Seinfeld, 2006). In that case, the dispersion effect enhances the Twomey effect. This trend is evident in in-situ measurements by Miles et al. (2000) and individual ship tracks in Lu et al. (2007).

ACPD
11, 15497–15550, 2011

2.3 Cloud thickness effect

The third term in Eq. (3), $d\ln H/d\ln N_a$, expresses the sensitivity of cloud thickness to changes in N_a, for which Wood (2007) derived an analytical formulation and applied a MLM to quantify the response of cloud thickness to perturbed N_d under different environmental conditions. Wood (2007) showed that the MSc cloud thickness response is determined by a balance between the moistening/cooling of the MBL resulting from precipitation suppression and drying/warming resulting from enhanced entrainment due to increased TKE. The drying and warming effect (cloud thinning) counteracts the moistening/cooling effect (cloud thickening). Also using the MLM model, Pincus and Baker (1994) predicted that cloud thickness (H) increases with N_d, especially at lower droplet concentration. Unlike the Pincus and Baker (1994) result that H is determined primarily by cloud top height, Wood (2007) found the cloud-base height to be the single most important determinant in affecting cloud thickness. If the cloud base height is lower (higher) than 400 m, increasing N_d leads to cloud thickening (thinning), which corresponds to LWP increase (decrease). The argument is that for an elevated cloud base, more evaporation occurs before precipitation reaches the surface, leading to two effects (Wood, 2007): (i) more sub-cloud evaporation limits the moistening/cooling of the MBL resulting from precipitation suppression, while allowing suppressed precipitation to increase the entrainment with increasing N_d, and (ii) sub-cloud evaporation has a stronger effect on turbulence than in-cloud latent heating; therefore enhanced sub-cloud evaporation increases the leverage of changes in cloud base precipitation on entrainment.

2.4 Diabaticity effect

The term, $d\ln f/d\ln N_a$, can be termed the diabaticity effect, accounting for the effect of liquid water depletion due to entrainment mixing and precipitation on cloud optical depth. This term cannot be evaluated separately from the other terms; the effect of diabaticity is intertwined with all the previous effects discussed. The qualitative effect

Discussion Paper | Discussion Paper | Discussion Paper | Discussion Paper |
ACPD
11, 15497–15550, 2011

of entrainment mixing on cloud behavior has been discussed in Sect. 1 (effects (c), (d), and (e)).

Some of these individual effects have been estimated in several previous studies (Table 2), including analytical solutions, in-situ measurements, satellite data, and LES. We will subsequently estimate the magnitudes for each effect from LES simulation.

3 Model description

3.1 Numerical model

In this study we employ the Weather Research and Forecasting (WRF) model V3.1.1 as a 3-D LES model. Several studies (e.g., Moeng et al., 2007; Wang and Feingold, 2009a,b; Wang et al., 2009) have used the WRF model for LES experiments and found the results are in good agreement with observations and other LES studies. Therefore we apply the WRF model as the LES dynamic framework. A detailed bin-resolved microphysical scheme (Geresdi, 1998; Rasmussen et al., 2002; Xue et al., 2010) is employed. In the bin microphysical scheme, aerosol number, cloud drop mass, and cloud drop number are computed over a size-resolved spectrum, predicting both cloud drop mass and number concentration following the moment-conserving technique (Tzivion et al., 1987, 1989; Reisin et al., 1996). Cloud drops are divided into 36 size bins with radii ranging from 1.56 µm to 6.4 mm and with mass doubling between bins. The masses for the first bin and the 36th bin are 1.5979×10^{-14} and 1.098×10^{-3} kg, respectively. In this study, the cutoff radius between cloud drop and rain drop size is taken to be ~40 µm. The aerosols are divided into 40 size bins between 0.006 to 66.2 µm.

3.2 Microphysical processes

The microphysical processes include aerosol activation, drop condensation/evaporation, collision-coalescence, collisional breakup, and sedimentation.

ACPD
11, 15497–15550, 2011

The aerosol size distribution is taken to be a single mode lognormal size distribution. Aerosol activation (or cloud droplet activation) occurs when the ambient supersaturation exceeds the critical supersaturation (S_c) for the given particle size. A hygroscopicity parameter κ, which describes the relationship between dry particle diameter and cloud condensation nuclei activity, is used to represent the composition-dependence of the solution water activity (Petters and Kreidenweis, 2007),

$$S_c(D) = \frac{D^3 - D_d^3}{D^3 - D_d^3(1-\kappa)} \exp\left(\frac{4\sigma_{\frac{s}{a}} M_w}{RT\rho_w D}\right) - 1, \tag{6}$$

where D is droplet diameter, D_d is aerosol dry diameter, $\sigma_{\frac{s}{a}}$ is the surface tension of the solution/air interface, M_w is the molecular weight of water, and ρ_w is the density of water. For the present study, the aerosol is assumed to be ammonium sulfate, for which κ is set to the constant value 0.615 (Petters and Kreidenweis, 2007).

The aerosol number concentration is held constant in the present study. The activated droplet number at each time is calculated by the difference between the particle number that would be activated at the diagnosed supersaturation and the pre-existing droplet number. Diffusional growth and evaporation of water drops are described following the vapor diffusion equation (Pruppacher and Klett, 1997). The Best and Bond number approach is used to calculate the terminal velocity of water drops (Pruppacher and Klett, 1997). The efficiencies of collision-coalescence between drops are derived using the data of Hall (1980) to calculate the kernel function. The collisional breakup of water drops is included following Feingold et al. (1988).

3.3 Other processes

Surface latent and sensible heat fluxes are calculated from local wind speed and the difference in specific humidity/potential temperature between the ocean and the air just above the ocean surface, following the Monin-Obukhov scheme. A 3-D turbulence scheme with 1.5-order turbulent kinetic energy (TKE) closure (Deardorff, 1980) is applied to prognose TKE. The Rapid Radiative Transfer Model (RRTM; Mlawer et al., 1997) with 16 LW bands is utilized to calculate LW radiative fluxes. The correlated-k method is used to simulate the cloud-top radiative cooling and heating rates. Shortwave radiation is represented using the Dudhia scheme (1989) to include solar flux, shortwave absorption and scattering in clear air, and reflection and absorption in cloud layers. A damping layer of 300 m thickness is employed in the upper boundary of domain for absorbing gravity wave energy to minimize the unphysical wave reflection off the upper boundary of the domain. Periodic boundary conditions in both x- and y- directions are assumed in the simulations. The monotonic flux limiter is applied to the basic advection scheme for scalar transport, as suggested by Wang et al. (2009) to avoid overestimates of cloud water and precipitation in cloud-scale simulations.

4 Experimental design

The WRF model with detailed bin microphysics is used to simulate an idealized MSc case for 30 hours to cover a diurnal cycle. The aerosol is assumed to be fully soluble ammonium sulfate following lognormal distribution with mean radius of 0.1 µm and geometric standard deviation of 1.5. The initial sounding profile for the control case (Fig. 1) is loosely based on the First International Satellite Cloud Climatology Project Regional Experiment (FIRE I; Duynkerke et al., 2004) in July 1987, with the total water mixing ratio decreased by 0.5 $\mathrm{g\,kg^{-1}}$ for a moderately drizzling (0.1–1 $\mathrm{mm\,day^{-1}}$) cloud. The case simulated is a shallow boundary layer with a depth of ~600 m and topped with a 12 K and $-3\,\mathrm{g\,kg^{-1}}$ temperature and moisture inversion, respectively. The Coriolis parameter is $8\times10^{-5}\,\mathrm{s^{-1}}$ (33.5° N, 119.5° W). Other initial conditions are similar to those in Hill et al. (2009). The nominal sea surface temperature (SST) is set to 288 K, and surface pressure is assumed to be constant at 1012.5 mb. The wind field is $-1\,\mathrm{ms^{-1}}$ in the x-direction and 6 $\mathrm{ms^{-1}}$ in the y-direction. The nominal large-scale divergence rate (D), $5.5\times10^{-6}\,\mathrm{s^{-1}}$, is given to prescribe the subsidence rate $W_{\mathrm{sub}} = -Dz$, where z is the

ACPD
11, 15497–15550, 2011

height above surface. The initial temperature field is perturbed pseudo-randomly by an amplitude of 0.1 K to accelerate the spinup of turbulence. Results are not sensitive to this amplitude. Both LW and SW radiation are considered. Radiative forcing is computed every time step. In order to avoid MSc dissipation due to strong solar radiation in summer, winter conditions are chosen for SW radiation.

Three Control simulations are performed within a 2.5 km×2.5 km×1.6 km domain for 30 h. The grid spacing is 20 m vertically and 50 m horizontally, with a 0.5 s time step. Aerosol number concentrations (N_a) of 100, 200, and 1000 cm^{-3} are taken to correspond to clean, semi-polluted, and polluted cases, respectively. For computational efficiency, sensitivity studies are performed over a smaller horizontal domain size, 1 km in x- and y-directions. Figure 2 shows that the cloud bulk properties of larger (2.5 km×2.5 km) and smaller (1 km×1 km) domain sizes are similar. Finer vertical spacing (10 m) is also examined, and the differences between results at higher and lower resolution are small. This agrees with the results of Hill et al. (2009) that LWP responses are insensitive to the resolution tests (grid size 20 m×20 m×10 m versus 40 m×40 m×20 m). Since our focus is on the directional changes of cloud properties in response to different ambient conditions, the smaller domain with 20 m vertical spacing is sufficient for sensitivity studies. Four significant environmental variables that control the structure of the MSc are considered: SST, free tropospheric water vapor mixing ratio (q_{ft}), large-scale divergence rate (D), and wind speed (U and V). The lower BL stability is controlled mainly by SST (Klein and Hartmann, 1993). The humidity above the BL determines the drying/warming effect through entrainment. The large-scale divergence D affects the subsidence rate. The wind speed is considered, as it affects the surface fluxes and the updraft velocity.

The simulations performed are listed in Table 3. In cases SST290 and SST292, SST is increased by 2 K and 4 K, respectively. In cases QFT3 and QFT1, the free tropospheric water vapor mixing ratio is decreased to 3.1 and 1.1 g kg^{-1}, respectively; the temperature profile remains unchanged. In cases DIV3 and DIV8, the large scale divergence rate is set to 3.0×10^{-6} and 8.0×10^{-6} s^{-1}, respectively, with all else unchanged.

ACPD
11, 15497–15550, 2011

In WIND case, the initial wind speed is set to $-4\,\mathrm{m\,s^{-1}}$ in the x-direction and $10\,\mathrm{m\,s^{-1}}$ in the y-direction for the entire boundary layer, stronger than the Control case. Both clean and polluted scenarios are simulated for each condition.

5 Results

5.1 Control case

The simulations start at 00:00 h local time. During the nighttime, cloud top LW radiative cooling generates a layer of negative buoyancy at cloud top (Fig. 3a), which enhances TKE and mixing, destabilizing the MBL. Enhancement of TKE increases the surface moisture flux (Fig. 4e) as well as cloud top entrainment. On balance, the increased surface moisture flux and the cloud top LW cooling outweigh the entrainment drying and warming, causing the cloud to thicken and LWP to increase at night (Fig. 4a, b). For the clean case ($N_a = 100\,\mathrm{cm^{-3}}$), measurable surface precipitation begins at 5 h as LWP increases, proceeding from light drizzle (<0.1 $\mathrm{mm\,day^{-1}}$) to moderate drizzle (0.1–1 $\mathrm{mm\,day^{-1}}$) after 7 h. During the daytime, the heating due to cloud absorption of solar radiation offsets LW cooling, decreasing the negative buoyancy and stabilizing the MBL. Internal heating of the cloudy layer via SW absorption acts to thin the cloud; surface precipitation is suppressed after 12 h (Fig. 4d). Also, the MSc becomes decoupled due to smaller TKE and less mixing, which is shown in the θ_l and q_t daytime profile (Fig. 3b, c), suggesting that the moister and cooler surface air is not transported to the cloud layer effectively (12–14 h). As the cloud continues to warm, the LWP decreases, attaining a minimum at ∼14 h.

After 14 h, cloud top height begins to increase again due to a decrease in downwelling SW radiation, leading to a cloud top predominantly defined by LW radiative cooling; and drizzle appears after ∼16 h (Fig. 4d). In the clean cloud, sedimentation causes the cloud base to lower as precipitation nears the surface. The larger droplets are able to sediment through the sub-cloud layer without evaporating thus leading to

ACPD
11, 15497–15550, 2011

the eventual dissipation of the cloud. The dissipation occurs under conditions of low N_a (and consequently, low N_d) (Fig. 4c) since the mean size of the droplets is higher in these cases, leading to more efficient removal of cloud water via precipitation. Moreover, these clouds are generally optically thin (Fig. 4f). Therefore cloud top LW cooling is rather small thus allowing subsidence to compress the MBL.

From clean to semi-polluted ($N_a = 200\,\mathrm{cm}^{-3}$) condition, precipitation is suppressed and LWP increases, due to more numerous and smaller cloud droplets; consequently, the collision-coalescence process is less efficient. Therefore, the semi-polluted cloud is nonprecipitating for the first 25 h. The precipitation suppression results in higher TKE, because in the presence of precipitation, (1) the latent heat releases from drizzle formation partially offsets the LW cooling, and (2) cooling from sub-cloud rain evaporation results in weaker turbulence intensity. As a result, the precipitation suppression accelerates the cloud-top entrainment, destabilizes the MBL, and establishes a well-mixed MBL. This is consistent with previous findings (e.g., Stevens et al., 1998; Lu and Seinfeld, 2005).

From 10 to 15 h, the semi-polluted cloud thins due to solar heating. Cloud base rise by 100 m while cloud top falls by 80 m since the base of the cloud is populated with more numerous smaller droplets that are more likely to evaporate in comparison to the droplets at cloud top. Consequently, LWP decreases. During the second night, the LWP of the semi-polluted cloud increases with weaker SW heating, exceeding $110\,\mathrm{g\,m}^{-2}$, and drizzle appears in the last 5 h of the simulation.

Proceeding from semi-polluted to polluted condition ($N_a = 1000\,\mathrm{cm}^{-3}$), stronger TKE is generated from sedimentation-entrainment and evaporation-entrainment by numerous smaller cloud droplets (as discussed previously in Sect. 1 pathway (d) and (e)), resulting in a drier cloud layer and less LWP, as compared to the semi-polluted cloud. This is evident from the vertical profile of vertical velocity variance ($(\overline{w'w'}$), a measure of strength of turbulent mixing, Fig. 3d). This result agrees with that of Ackerman et al. (2004), in that the entrainment increases with increasing N_a in all simulations. And the LWP is lower in the polluted cloud than in the semi-polluted cloud for the 30 h duration

ACPD
11, 15497–15550, 2011
Aerosol-cloud-precipitation interactions in MSc
Y.-C. Chen et al.

(Fig. 4a). After 15 h, as in the case of the semi-polluted cloud, the well-mixed MBL is restored through enhanced LW cooling and TKE, and the cloud grows even thicker than during the first night. Compared to the clean case, in the absence of precipitation the MSc lifetime increases, as suggested by Albrecht (1989).

In Fig. 4f, the cloud optical depth, τ, is calculated by

$$\tau = \int\int 2\pi r^2 n(r)\, dr\, dz, \tag{7}$$

where the extinction efficiency is approximately 2 at visible wavelengths for the typical size of cloud drops (Seinfeld and Pandis, 2006), and $n(r)$ is the droplet number concentration distribution. It is shown that the cloud optical depth increases with N_a (Fig. 4f), with larger enhancement at night than during the daytime. During the 30 h simulation, cloud optical depth, as well as LWP, precipitation, and cloud fraction exhibit a strong diurnal variation (Fig. 4). The cloud fraction remains 100 % for semi-polluted and polluted clouds except from 12 to 14 h when SW heating is strongest. However, under clean condition, with both precipitation and solar heating, cloud fraction decreases significantly (Fig. 4g). And as a result of more pronounced entrainment, the polluted cloud is warmer and drier than the clean and semi-polluted clouds (Fig. 3b, c).

The overall effect (Control cases) of changes in N_a can be summarized as follows: (1) with non/light drizzle (<0.1 mm day^{-1}), increase in N_a results in stronger entrainment and thus lower LWP; and (2) with moderate/heavy drizzle (>0.1 mm day^{-1}), increase in N_a results in precipitation suppression, and thus higher LWP. For the diurnal variation, nighttime LWP is larger than daytime LWP, a result of cloud thinning and decoupling during daytime. Overall, cloud optical depth τ increases with increased N_a (Fig. 4f). These effects are consistent with the studies listed in Table 1.

ACPD
11, 15497–15550, 2011

5.2 Sensitivity to environmental conditions

5.2.1 Effects of SST – SST290 and SST292 cases

First, we examine the effect of a higher SST on the response of the MSc to perturbations in aerosol concentration. As SST increases, the surface fluxes increase accordingly with higher SST (Fig. 5c, g), causing the cloud top temperature inversion strength to be weakened and cloud top to rise. Also, the cloud base rises due to higher SST and thus higher lifting condensation level. Overall, cloud base rises more than cloud top, resulting in a thinner cloud (Fig. 5b), consistent with the short time scale responses in Lu and Seinfeld (2005). In SST290 and SST292 clean clouds, the precipitation is suppressed (Fig. 5d) because of a thinner cloud and lower LWP. During the daytime, the cloud thickness is constrained by both solar absorption and the warmer MBL. The cloud layer, gradually warmed by solar heating and higher MBL temperature, becomes more stable and decouples from the surface. In the second night, the LW radiation enhances the turbulence and MBL overturning, and a well-mixed state is re-established, causing the cloud to thicken. The precipitation in SST290 clean cloud initiates at ~20 h, and with moderate drizzling rate (0.1–1 mm day^{-1}) after 21 h, the cloud becomes very thin in the end of simulation. While in SST292 clean cloud, lower LWP prevents the cloud from drizzling, and it keeps thickening in the second night.

In SST290 and SST292 polluted clouds, the numerous and smaller cloud droplets evaporate more efficiently under higher temperature, and the cloud dissipates at ~14 h with the existence of strong solar radiation. With the onset of the second night, the LW-driven TKE enhances the vertical advection of water vapor, gradually replenishing moisture at the lifting condensation level. And the cloud reforms at ~20 and 27 h for SST290 and SST292 polluted cases, respectively (Fig. 5f).

The overall effect of an increasing SST can be summarized as follows: (1) when SST is increased compared to the Control case, the simulated cloud thins and LWP decreases on a short time scale (several hours); and (2) when SST is increased and N_a is increased, entrainment effects are more pronounced and LWP decreases.

ACPD
11, 15497–15550, 2011

5.2.2 Effects of free tropospheric humidity – QFT3 and QFT1 cases

As the free tropospheric air becomes drier, the larger discontinuity in humidity between the MBL and the free troposphere results in stronger evaporative cooling in the cloud top inversion region. This enhances the TKE, leads to stronger mixing, and increases both cloud top entrainment and upward surface fluxes. Compared to the Control case, the enhanced cloud top entrainment leads to a deeper MBL as well as stronger drying. As a result, both the cloud top and base rise (Fig. 6b, f), with the cloud base rising more, thus resulting in a thinner cloud.

In the QFT3 case, the increased surface moisture flux compensates for the drying from enhanced entrainment, and the cloud thickens at night. However in the QFT1 case, the cloud thins from the outset as drying from entrainment mixing exceeds the moistening from the surface flux (Fig. 6a, e). In the QFT3 clean case, the precipitation occurs after 20 h, with heavier drizzle (>0.1 mm day^{-1}) occurring after 21 h. The cloud eventually dissipates by the end of simulation. On the other hand, the lower LWP in the QFT1 clean case prevents the cloud from precipitating during the 30 h duration. In the second night, the cloud deepens as the surface moisture flux outweighs the drying by entrainment, and LWP gradually increases. Among all the clean cases, QFT1 is the only one in which the cloud exists at the end of the simulation. Compared to the QFT1 polluted case, LWP is higher in the clean cloud than in the polluted cloud within the 30 h duration.

The overall effect of a drier free troposphere can be summarized as follows: (1) when q_{ft} is decreased compared to the Control case, the cloud thins and LWP decreases on a short time scale; and (2) when q_{ft} is decreased and N_{a} is increased, entrainment effects are significant and LWP decreases.

5.2.3 Effects of large-scale divergence – DIV3 and DIV8 Cases

Changes in the large-scale divergence rate mainly affect the cloud top height. As the large-scale divergence weakens (DIV3), the cloud height increases, and the cloud

ACPD
11, 15497–15550, 2011

thickens. In the DIV3 clean cloud, this results in earlier and heavier precipitation than in the Control case (Fig. 7d). During the first night, precipitation initiates at ~4 h with maximum rate ~0.45 mm day^{-1}. During the day, LWP decreases, reaching a minimum at ~14 h (Fig. 7a), the same as in the Control case. The cloud thickens again afterwards as the SW heating decreases. Due to the lower cloud layer in the second evening (Fig. 7b), precipitation droplets are less likely to evaporate before reaching the surface, causing heavier surface precipitation to occur between 16 and 21 h, with maximum rate 1.2 mm day^{-1}, and eventually the cloud dissipates at ~22 h.

In the DIV3 polluted case, the cloud thickens with the LWP reaching ~150 g m^{-2} during the first night, as compared to ~100 g m^{-2} in the Control case (Fig. 7e). Entrainment is weaker in this scenario owing to weaker large-scale subsidence. During the second night, the cloud grows even thicker, with LWP >200 g m^{-2} at the end of the simulation, showing that with a weaker subsidence rate, the polluted cloud can keep growing without being strongly capped.

In the DIV8 case, on the other hand, the cloud becomes thinner due to stronger "capping" from the air above. In the DIV8 clean case, lower LWP inhibits precipitation during the first night. Compared to the DIV3 and Control clean clouds, the cloud dissipates later due to later onset and lighter drizzle. In the DIV8 polluted case, however, the cloud disappears due to stronger subsidence and efficient evaporation during the daytime. It is shown that when the subsidence rate is increased, the cloud thins due to a decrease in cloud top height and is even able to dissipate completely.

The overall effect of the large-scale divergence rate can be summarized as follows: (1) when D is decreased compared to the Control case, the cloud thins and LWP decreases on a short time scale; and (2) when D is increased (decreased) and N_a is increased, stronger entrainment (precipitation suppression) leads to lower (higher) LWP.

ACPD
11, 15497–15550, 2011

5.2.4 Effects of wind speed – WIND Cases

Stronger wind (U and V are −4 and 10 ms^{-1}, respectively; compared to −1 and 6 ms^{-1} in Control case) increases the surface latent heat fluxes, resulting in slightly higher LWP than in the Control case, and thus more precipitation in the clean cloud (Fig. 8d). Stronger sedimentation lowers the cloud top and base relative to the Control case (Fig. 8b). In the afternoon, the LWP increases and heavy drizzle occurring in the clean case causes the cloud to disappear at ∼21 h, earlier than that in the Control clean case. This is a result of significant water loss due to low cloud base. In the polluted case, on the other hand, it shows similar diurnal variation as the Control case (Fig. 8f), but with higher LWP than the Control case at night. It is shown that within the range simulated, the cloud response is not very sensitive to the wind speed compared to other environmental variables.

The overall effect of stronger wind speed can be summarized as follows: (1) when U, V are increased compared to the Control case, the cloud thickens and LWP increases, resulting in heavier precipitation (short time scale); and (2) when U, V are increased and N_a is increased, precipitation is suppressed and LWP is higher.

5.3 LWP differences between clean and polluted cases

The LWP difference between the polluted and clean cloud (ΔLWP) for all cases is shown in Fig. 9 (after 16 h the cloud dissipates in some cases). For Control, DIV3 and WIND cases, LWP is higher under polluted conditions (ΔLWP>0). This is because under these moister conditions with heavier precipitation, as the aerosol number concentration increases, precipitation is suppressed, resulting in less water loss and higher LWP. The maximum ΔLWP reaches 70 gm^{-2} in the DIV3 case, whereby heavier precipitation occurs in the clean cloud. In contrast, the other cases (SST290, SST292, DIV8, QFT3 and QFT1 case) have lower LWP in the polluted cloud than the clean cloud (ΔLWP<0), which shows that in the absence of precipitation or with light drizzle, the evaporation-entrainment effect and sedimentation-entrainment effect are pronounced

ACPD
11, 15497–15550, 2011

in the polluted cloud, causing LWP to decrease. The minimum ΔLWP is ∼−28 $\mathrm{g\,m^{-2}}$ in the QFT1 case, showing that the drier the free troposphere, the stronger the entrainment effect. Overall, LWP is found to be more sensitive to precipitation than to entrainment.

5.4 Relation of LES experiments to analytical approximation

Equation 3 is an approximate analytical expression relating changes in N_a to changes in various cloud properties. Here we attempt to estimate the sign and relative magnitude of each term in Eq. (3) using the LES experiments. To evaluate the derivatives we use finite differences, ΔN_a, to represent dN_a, using N_a values of 100, 200, 500 and 1000 $\mathrm{cm^{-3}}$. As noted earlier, while the diabaticity effect, $d(\ln f)/d(\ln N_a)$, is expressed separately in Eq. (3), this effect cannot easily be separated numerically from the others in Eq. (3). Therefore, $\Delta \ln N_d/\Delta \ln N_a$ is estimated rather than $\Delta \ln N_{ad}/\Delta \ln N_a$; and the estimation of $\Delta \ln k/\Delta \ln N_a$ and $\Delta \ln H/\Delta \ln N_a$ already incorporates the diabaticity effect. Control, SST290, QFT3, and DIV3 cases are considered to evaluate each term. The relationship of τ, N_d, k, and H to N_a are calculated by conditionally-averaging over the cloudy fraction of the domain. Nighttime (4–7 h) and daytime (12–15 h) are discussed separately (Fig. 10).

5.4.1 Twomey effect

The estimated value of $\Delta \ln N_d/\Delta \ln N_a$ is within the range of 1.00–1.25 at night (4–7 h) and 0.83–1.37 during the day (12–15 h) (Table 4), with a lower value in SST290 and QFT3 cases than in Control and DIV3 cases, a result of a drier atmosphere and lower supersaturation, and thus lower N_d. During the daytime, N_d is lower than that at nighttime due to solar heating (Fig. 10), and the values of $\Delta \ln N_d/\Delta \ln N_a$ are more scattered. Compared to other studies (Table 2), the estimated magnitude of $\Delta \ln N_d/\Delta \ln N_a$ is higher, as compared to the range of 0.6 to 0.9 based on Eqs. (4) and (5).

ACPD
11, 15497–15550, 2011

5.4.2 Dispersion effect

The coefficient k is calculated (Martin et al., 1994; Lu and Seinfeld, 2006) as a function of relative dispersion (d) and skewness (s) of the droplet number concentration distribution $n(r)$,

$$k = \frac{\left(1+d^2\right)^3}{\left(sd^3+1+3d^2\right)^2}, \tag{8}$$

where $d = \sigma/\bar{r}$, $\bar{r}$ is mean droplet radius, σ is the standard deviation of droplet spectrum, given by

$$\sigma = \left(\frac{1}{N_\mathrm{d}}\int (r-\bar{r})^2 n(r)dr\right)^{1/2}, \tag{9}$$

and skewness s is defined as

$$s = \frac{1}{\sigma^3 N_\mathrm{d}}\int (r-\bar{r})^2 n(r)dr. \tag{10}$$

Calculated over the cloud and drizzle spectra, the range of k from the simulations is within 0.58 and 0.85 (Fig. 10). During the daytime, k is smaller than at night, suggesting that the evaporation of cloud droplets due to SW heating results in a more dispersed droplet spectrum and smaller k. Also, the estimated $\Delta\ln k/\Delta\ln N_\mathrm{a}$ at nighttime is smaller for the drier cases (SST290 and QFT3), and larger for the moister case (DIV3). In the DIV3 case with stronger precipitation, $\Delta\ln k/\Delta\ln N_\mathrm{a}$ accounts for 10 % of total cloud susceptibility, larger than in other cases with less precipitation; this result is consistent with Lu and Seinfeld (2006), where smaller value of $\Delta\ln k/\Delta\ln N_\mathrm{a}$ occurs for the cloud with weaker drizzle, and larger value with stronger precipitation. This is because with increased N_a, there is less spectral broadening due to suppressed collision-coalescence. Also, spectral narrowing occurs via condensational growth in regions of

Discussion Paper | Discussion Paper | Discussion Paper | Discussion Paper |

ACPD
11, 15497–15550, 2011

higher updraft velocities because suppressed precipitation leads to stronger TKE. The positive correlation of k to N_a is consistent with Miles et al. (2000) and individual ship tracks in Lu et al. (2007), yet opposite to that obtained by other flight-averaged data (Martin et al., 1994, Liu and Daum, 2002; ensemble cloud averages in Lu et al., 2007).

Lu et al. (2007) found that on the ensemble-averaged cloud scale (~several tens of kilometers), an increase in N_a results in spectral broadening (smaller k), because for the flight-averaged data, the relationship between k and N_a is affected not only by N_a but also by various meteorological conditions in different sampling locations. The meteorological differences thus affect the dynamical factors, such as entrainment mixing, updraft velocity, drizzle strength, etc, which accordingly change the dispersion width. Therefore for the flight-averaged observational data, the clean and polluted clouds were not necessarily subject to the same sounding (Lu et al., 2007), which causes the k-N_a relationship to be affected by factors other than simply changes in N_a. While on the scale of a cloud perturbed by a single ship track, spectral narrowing (larger k) occurs in response to increased N_a, for which the ship track and clean regions are embedded in the same sounding. In this LES study, with the ambient conditions being fixed, the environment is identical, and the aerosol-induced dispersion changes can therefore be distinguished and separated from other meteorological factors.

5.4.3 Cloud thickness effect

Aerosols exert the main influence on cloud thickness through precipitation efficiency, radiation, and cloud dynamics (entrainment). The estimated $\Delta \ln H/\Delta \ln N_a$ at nighttime is slightly negative (~−0.01 to −0.04) within the range of simulated environmental conditions (Table 4), except for the DIV3 case ($\Delta \ln H/\Delta \ln N_a = 0.014$) in which stronger drizzle occurs in the clean case, causing H to increase with increasing N_a, a result of precipitation suppression. As N_a increases from 200 to 1000 cm^{-3}, $\Delta \ln H/\Delta \ln N_a$ is negative in all cases (Fig 10) as a result of evaporation-entrainment and sedimentation-entrainment effects. During the daytime, H is smaller and the values of $\Delta \ln H/\Delta \ln N_a$ is more scattered than at night. The sign of $\Delta \ln H/\Delta \ln N_a$ is consistent with Lu and Se-

ACPD
11, 15497–15550, 2011

infeld (2005) (Table 2), where $\partial \ln LWP/\partial \ln N_a$ is negative, with a larger impact under clean background. Overall, though the magnitude of $\Delta(\ln H)/\Delta(\ln N_a)$ is small compared to that of $\Delta(\ln N_d)/\Delta(\ln N_a)$ (Table 4), with the coefficient 5 in Eq. (3), the effect is enhanced. The cloud thickness effect is the only one that exhibits either positive or negative magnitude, which enhances or counteracts other effects.

5.4.4 Cloud optical depth susceptibility

Cloud optical depth is calculated following Eq. (7). As N_a increases from 100 to 1000 cm^{-3}, the estimated value of $\Delta\ln\tau/\Delta\ln N_a$ lies between 0.28 and 0.53 at night, with higher value in the DIV3 case and lower value in the SST290 and QFT3 cases (Table 4). This suggests that with a moister atmosphere and heavier precipitation, $\Delta\ln\tau/\Delta\ln N_a$ is larger. Also, $\Delta\ln\tau/\Delta\ln N_a$ is larger at lower N_a. In the nighttime Control case, as N_a doubles from 100 to 200 cm^{-3}, $\Delta\ln\tau/\Delta\ln N_a$ is more than two times larger than that when doubling N_a from 500 to 1000 cm^{-3} (0.54 versus 0.24), suggesting that cloud susceptibility is stronger under lower N_a. Therefore, the enhancement of cloud susceptibility is more pronounced when increasing N_a from a clean background.

During the daytime, the magnitude of τ is lower as a result of solar heating and cloud thinning (Fig. 10). The magnitude of $\Delta\ln\tau/\Delta\ln N_a$ lies between −0.36 and 0.63, more scattered than that of the nighttime (0.28–0.53). Because the MBL decouples and the cloud thins significantly during the day, the evaluation which is based on only cloudy grids has a larger standard deviation and should be viewed with more caution. In the SST290 case, $\Delta\ln\tau/\Delta\ln N_a$ is actually negative during the day, a result of cloud dissipation under polluted case. With higher temperature, cloud droplet evaporation during the day causes the cloud to disappear (Fig. 5f).

Comparing $\Delta\ln\tau/\Delta\ln N_a$ from LES simulation (Eq. 7) and from Eq. (3), it is seen that the two values are in good agreement to each other (Fig. 11). The difference between these two estimated $\Delta\ln\tau/\Delta\ln N_a$ value lies within the margin of error (standard deviation), with the largest discrepancy occurring in daytime SST290 case. Note that the

Discussion Paper | Discussion Paper | Discussion Paper | Discussion Paper |

ACPD

11, 15497–15550, 2011

Aerosol-cloud-precipitation interactions in MSc

Y.-C. Chen et al.

standard deviation is larger for daytime SST290, showing the value is less representative than in other cases. The relatively close agreement between the LES simulation and analytical expression in Eq. (3) was not necessarily to be expected. The analytical formulation can therefore be treated as a good approximation of cloud optical depth susceptibility.

Considering the significance of each term in contributing to the cloud susceptibility $\Delta \ln \tau / \Delta \ln N_a$, the Twomey effect $\Delta \ln N_d / \Delta \ln N_a$ is the dominant term, contributing over 85 % of the total effect during the nighttime. The dispersion effect accounts for 3 % to 10 % of the total effect at night, and the cloud thickness effect accounts for 5 % to 22 % of the overall effect, acting to diminish or enhance the Twomey effect. During daytime the ranges of values are more scattered due to the MBL decoupling and significant cloud thinning.

5.4.5 Ratio of indirect effects

Ignoring the dispersion and diabaticity effects, Eq. (3) can be rewritten as:

$$\frac{d \ln \tau}{d \ln N_a} = \frac{1}{3}\left(\frac{d \ln N_d}{d \ln N_a} + 5\frac{d \ln H}{d \ln N_a}\right). \quad (11)$$

One can define the ratios of the cloud thickness effect to the Twomey effect, that is, $R_{IE} = 5(\frac{\Delta \ln H}{\Delta \ln N_d})$ (Wood, 2007). A value of $R_{IE} = 1$ corresponds to the cloud thickness effect doubling the Twomey effect, and $R_{IE} = -1$ implies a complete cancellation the Twomey effect. In Wood (2007), with given environmental forcing, the MLM determines the equilibrium state of the MBL. And by perturbing N_d by 5 %, the analytical response indicates that R_{IE} is strongly tied to cloud base height on a short time scale (0–8 h); and only when the cloud base height is very low does the cloud thickness effect overweigh the Twomey effect.

In this study we perform an examination similar to that of Wood (2007) by doubling the aerosol concentration from 100 to 200 cm^{-3}. Here R_{IE} is calculated by $5(\frac{\Delta \ln H}{\Delta \ln N_a} / \frac{\Delta \ln N_d}{\Delta \ln N_a})$ from the LES simulation, and the value is averaged over 4–7 h for 27

ACPD
11, 15497–15550, 2011

cases, covering the variables and values listed in Table 5. The cloud base height and cloud thickness under the unperturbed case are averaged during the same period for N_a 100 cm^{-3}. Fig. 12a demonstrates a similar trend in R_{IE} as that shown by Wood (2007) (Fig. 8a). With higher cloud base, R_{IE}<0, and vice versa.

The positive R_{IE} appears only in Control and DIV3 cases, where the moister environment leads to lower cloud base and stronger precipitation in the unperturbed (N_a 100 cm^{-3}) condition. The other cases have negative R_{IE}, suggesting the cloud thickness effect offsets the Twomey effect. In a drier environment, the cloud base is higher, and thus less precipitation occurs under clean conditions. With increased aerosol, the enhanced entrainment effect therefore results in a thinner cloud and negative cloud thickness effect. The lowest R_{IE} (−1.47) appears under the driest condition (in which SST is 292 K, D is 8×10^{-6} s^{-1}, and q_{ft} is 1.1 g kg^{-1}). The relationship between R_{IE} and cloud thickness (Fig. 12b) also shows a positive correlation; a thicker cloud corresponds to a larger R_{IE}, and vice versa.

Environmental conditions that favor higher cloud bases are those of higher SST and a drier free troposphere, consistent with results of Wood (2007). Variation in large-scale divergence affects the cloud top height, but not the cloud base height, therefore R_{IE} under difference divergence rates is independent of cloud base height.

6 Conclusions

Aerosol-cloud-precipitation interactions, which involve aerosol and cloud microphysics, atmospheric dynamics, and radiation, are complex and intertwined. We report here on a comprehensive numerical study of the dynamical response of MSc to changes in aerosol number concentration N_a using the WRF model with a detailed bin-resolved microphysical scheme as a three-dimensional LES model. Simulations are performed to explore the cloud diurnal responses to varied aerosol number concentration and different meteorological conditions (SST, free-tropospheric water vapor mixing ratio, large-scale subsidence, and wind speed). Based on the LES simulations, the magnitude and sign of the Twomey effect, droplet dispersion effect, cloud thickness effect, and cloud susceptibility are evaluated and compared to approximate analytical expressions that have been previously derived.

For moderate/heavy drizzling (>0.1 mm day^{-1}) clouds, increase in N_a suppresses precipitation, causing the LWP to increase. For non/light drizzling (<0.1 mm day^{-1}) clouds, an increase in N_a leads to numerous smaller cloud droplets, reducing the sedimentation, increasing the evaporation at cloud top, resulting in larger TKE, stronger entrainment, and LWP reduction. These are termed as sedimentation-entrainment and evaporation-entrainment effects. In daytime, SW heating offsets LW cooling, causing the cloud to thin, and reduced turbulent mixing results in a decoupled MBL. Over the 30 h duration, the precipitating cloud under clean background disappears due to water loss, whereas the semi-polluted and polluted clouds continue to thicken. The dominant physical/dynamical mechanisms due to aerosol perturbations differ for moderate/heavy drizzling and non/light drizzling MSc.

Considering different environmental conditions, the simulated cloud responses are generally consistent with previous studies. Under higher SST, drier free-troposphere, or stronger large scale divergence rate, the clouds become thinner than in the Control case, and precipitation decreases. Higher SST causes both cloud top and base heights to increase, with cloud base being lifted more, resulting in a thinner cloud. Lower free-tropospheric humidity leads to stronger evaporation-entrainment, and therefore higher TKE and deeper MBL. Also, the entrainment dries the air, causing the cloud base to be higher. Overall, the cloud base elevates more than does the cloud top, thus creating a thinner cloud. Under stronger large scale subsidence, the cloud top is prohibited from rising; consequently the lower cloud top makes the cloud thinner. Under stronger wind speed, the enhanced surface fluxes moisten the MBL, thicken the cloud, and increase precipitation.

An analytical formulation of cloud susceptibility to aerosol perturbations can be expressed by the sum of the Twomey, droplet dispersion, cloud thickness, and diabaticity effects. Control, SST290, QFT3, and DIV3 cases covering N_a values of 100, 200, 500, and 1000 cm^{-3} are utilized to evaluate each effect for both nighttime and daytime conditions. The estimated Twomey effect is the dominant term in the total cloud susceptibility and is larger under moister ambient conditions. The sign of the droplet dispersion effect is positive; it is larger for heavier drizzling cases (Control and DIV3), and smaller for non/light drizzling cases (SST290 and QFT3). The dispersion effect plays a minor role in the total cloud susceptibility, accounting for 3–10 % at night. The cloud thickness effect is negative in all cases, expect in DIV3 case, where stronger precipitation occurs in clean case, and thus an increase in N_a suppresses precipitation, causing the cloud to thicken. The drier the environment, the smaller the magnitude of $\Delta(\ln H)/\Delta(\ln N_a)$; the same trend as in the other effects. The cloud thickness effect is the only one that can reduce the total cloud susceptibility through cloud thinning.

The estimated magnitude of the cloud susceptibility, $\Delta(\ln\tau)/\Delta(\ln N_a)$, is between 0.28 and 0.53 at nighttime, with larger magnitude for heavier drizzling cases and smaller magnitude for non/light drizzling cases. Thus $\Delta(\ln\tau)/\Delta(\ln N_a)$ is more pronounced under a moister environment with stronger precipitation. Also, the cloud susceptibility is larger in a cleaner background. Comparing the cloud susceptibility derived directly from LES results and that calculated based on each individual effect in analytical formulation, there is good agreement, with the difference being within the error bar (Fig. 11). This indicates that the analytical expression is a useful form to evaluate the cloud susceptibility with reasonable accuracy. In daytime, the range of magnitude of each effect is more scattered as compared to nighttime. Because the MBL decouples and the cloud thins during the day, the evaluation which is based on only cloudy grids has a larger standard deviation should be viewed with more caution. Overall, however, the magnitude of each term during the daytime is larger for moderate/heavy drizzling conditions, consistent with the nighttime tendency.

ACPD
11, 15497–15550, 2011

The ratio of the cloud thickness effect to the Twomey effect (R_{IE}) is examined. It is found in a short time scale, the ratio depends on cloud base height and cloud thickness in the unperturbed clouds. For thicker clouds with stronger precipitation and lower cloud base, the cloud thickness effect enhances the Twomey effect. On the other hand, for drier cases with less precipitation and higher cloud base, they tend to have negative R_{IE}, showing that the cloud thickness effect diminishes the Twomey effect. In the simulated cases, R_{IE} is negative for most cases, showing that when there is non/light precipitation, the cloud thickness effect counteracts the Twomey effect.

Acknowledgements. This work was supported by office of Naval Research grant N00014-10-1-0200. YCC thanks Frank Li, Adrian Hill, and Andreas Zuend for helpful suggestions. LX acknowledges the support of the Advanced Study Program at NCAR. HW thanks the Fund for Innovative Climate and Energy Research (FICER) at the University of Calgary. Computations were carried out on the CITerra Dell Cluster of the Geological and Planetary Sciences Division at Caltech.

References

Ackerman, A. S., Toon, O. B., Taylor, J. P., Johnson, D. W., Hobbs, P. V., and Ferek, R. J.: Effects of aerosols on cloud albedo: Evaluation of Twomey's parameterization of the cloud susceptibility using measurement of ship tracks, J. Atmos. Sci., 57, 2684–2695, 2000. 15506, 15535

Ackerman, A. S., Kirkpatrick, M. P., Stevens, D. E., and Toon, O. B.: The impact of humidity above stratiform clouds on indirect aerosol climate forcing, Nature, 432, 1014–1017, 2004. 15501, 15502, 15503, 15513, 15534

Ackerman, A. S., vanZanten, M. C., Stevens, B., Savic-Jovcic, V., Bretherton, C. S., Chlond, A., Golaz, J.-C., Jiang, H., Khairoutdinov, M., Krueger, S. K., Lewellen, D. C., Lock, A., Moeng, C.-H., Nakamura, K., Petters, M. D., Snider, J. R., Weinbrecht, S., and Zulauf, M.: Large-eddy simulations of a drizzling, stratocumulus-topped marine boundary layer, Mon. Weather Rev., 137, 1083–1110, doi:10.1175/2008MWR2582.1, 2009. 15500

Albrecht, B.: Aerosols, Cloud Microphysics, and Fractional Cloudiness, Science, 245, 1227–1230, doi:10.1126/science.245.4923.1227, 1989. 15500, 15514

ACPD

11, 15497–15550, 2011

Brenguier, J.-L., Pawloska, H., Schüller, L., Preusker, R., and Fischer, J.: Radiative properties of boundary layer clouds: Droplet effective radius versus number concentration, J. Atmos. Sci., 57, 803–821, 2000. 15504

Bretherton, C. S. and Wyant, M. C.: Moisture transport, lower troposphere stability, and decoupling of cloud-topped boundary, J. Atmos. Sci., 54, 148–167, 1997. 15499

Bretherton, C. S., Macvean, M. K., Bechtold, P., Chlond, A., Cotton, W. R., Cuxart, J., Cuijpers, H., Khairoutdinov, M., Kosovic, B., Lewellen, D., Moeng, C.-H., Siebesma, P., Stevens, B., Stevens, D. E., Sykes, I., and Wyant, M. C.: An intercomparison of radiatively driven entrainment and turbulence in a smoke cloud, as simulated by different numerical models, Q. J. Roy. Meteorol. Soc., 125, 391–423, 1999. 15500

Bretherton, C. S., Blossey, P. N., and Uchida, J.: Cloud droplet sedimentation, entrainment efficiency, and subtropical stratocumulus albedo, Geophys. Res. Lett., 34, L03813, doi:10.1029/2006GL027648, 2007. 15500, 15501

Caldwell, P. and Bretherton, C. S.: Response of a subtropical stratocumulus-capped mixed layer to climate and aerosol changes, J. Climate, 22, 20–38, 2009a. 15499, 15502, 15534

Caldwell, P. and Bretherton, C. S.: Large eddy simulation of the diurnal cycle in Southeast Pacific stratocumulus, J. Atmos. Sci., 66, 432–449, 2009b. 15500

Chlond, A. and Wolkau, A.: Large-eddy simulation of a nocturnal stratocumulus-topped marine atmospheric boundary layer: An uncertainty analysis, Bound-Lay. Meteorol., 95, 31–55, 2000. 15500

Deardorff, J.: Stratocumulus-capped mixed layers derived from a three dimensional model, Bound-Lay. Meteorol., 18, 495–527, 1980. 15510

Duynkerke, P. G., de Roode, S. R., van Zanten, M. C., Calvo, J., Cuxart, J., Cheinet, S., Chlond, A., Grenier, H., Jonker, P. J., Kohler, M., Lenderink, G., Lewellen, D., Lappen, C.-L., Lock, A. P., Moeng, C.-H., Muller, F., Olmeda, D., Piriou, J.-M., Sanchez, E., and Sednev, I.: Observations and numerical simulations of the diurnal cycle of the EUROCS stratocumulus case, Q. J. Roy. Meteorol. Soc., 604, 3269–3296, 2004. 15500, 15510

Feingold, G. and Chuang, P. Y.: Analysis of the influence of filmforming compounds on droplet growth: Implications for cloud microphysical processes and climate, J. Atmos. Sci., 59, 2006–2018, 2002. 15506

Feingold, G., Tzivion, S., and Levin, Z.: Evolution of raindrop spectra. Part I: solution to the stochastic collection/breakup equation using the method of moments, J. Atmos. Sci., 45, 3387–3399, 1988. 15509

ACPD

11, 15497–15550, 2011

Aerosol-cloud-precipitation interactions in MSc

Y.-C. Chen et al.

Geresdi, I.: Idealized simulation of the Colorado hailstorm case: comparison of bulk and detailed microphysics, Atmos. Res., 45, 237–252, 1998. 15508

Hall, W. D.: A detailed microphysical model within a two-dimensional framework: Model description and preliminary results, J. Atmos. Sci., 37, 2486–2507, 1980. 15509

Hill, A. A., Dobbie, S., and Yin, Y.: The impact of aerosols on non-precipitating marine stratocumulus., Q. J. Roy. Meteorol. Soc., 134, 1143–1154, doi:10.1002/qj.278, 2008. 15500, 15501, 15502, 15534

Hill, A. A., Feingold, G., and Jiang, H.: The influence of entrainment and mixing assumption on aerosol-cloud interactions in marine stratocumulus, J. Atmos. Sci., 66, 1450–1464, 2009. 15500, 15501, 15510, 15511, 15534, 15535

IPCC: Summary for Policymakers, in: Climate Change 2007: The Physical Science Basis. Contribution of Working Group I to the Fourth Assessment Report of the Intergovernmental Panel on Climate Change, edited by: Solomon, S., Qin, D., Manning, M., Chen, Z., Marquis, M., Averyt, K. B., Tignor, M., and Miller, H. L., Cambridge University Press, New York, NY, USA, 989 pp., 2007. 15499

Jiang, H., Feingold, G., and Cotton, W. R.: Simulations of aerosol-clouddynamical feedbacks resulting from entrainment of aerosol into the marine boundary layer during the Atlantic Stratocumulus Transition Experiment, J. Geophys. Res., 107, 4813, doi:10.1029/2001JD001502, 2002. 15500

Klein, S. A. and Hartmann, D. L.: The seasonal cycle of low stratiform clouds, J. Climate, 6, 1588–1606, 1993. 15511

Lilly, D. K.: Models of cloud topped mixed layers under a strong inversion, Q. J. Roy. Meteorol. Soc., 94, 292–309, 1968. 15499

Lilly, D. K.: Entrainment into mixed layers. Part II: A new closure, J. Atmos. Sci., 59, 3353–3361, 2002. 15499

Liu, Y. G. and Daum, P. H.: Anthropogenic aerosols: Indirect warming effect from dispersion forcing, Nature, 419, 580–581, 2002. 15506, 15521

Lu, M. and Seinfeld, J. H.: Study of the aerosol indirect effect by large-eddy simulation of marine stratocumulus, J. Atmos. Sci., 62, 3909–3932, 2005. 15500, 15501, 15502, 15503, 15513, 15515, 15521, 15534, 15535

Lu, M. and Seinfeld, J. H.: Effect of aerosol number concentration on cloud droplet dispersion: A large-eddy simulation study and implications for aerosol indirect forcing, J. Geophys. Res., 111 D02207, doi:10.1029/2005JD006419, 2006. 15500, 15506, 15520, 15535

ACPD
11, 15497–15550, 2011

Aerosol-cloud-precipitation interactions in MSc

Y.-C. Chen et al.

Title Page
Abstract Introduction
Conclusions References
Tables Figures
◀| |▶
◀ ▶
Back Close
Full Screen / Esc
Printer-friendly Version
Interactive Discussion

Lu, M.-L., Conant, W. C., Jonsson, H. H., Varutbangkul, V., Flagan, R. C., and Seinfeld, J. H.: The Marine Stratus/Stratocumulus Experiment (MASE): Aerosol-cloud relationships in marine stratocumulus, J. Geophys. Res., 112, D10209, doi:10.1029/2006JD007985, 2007. 15506, 15521

Martin, G. M., Johnson, D. W., and Spice, A.: The measurement and parameterization of effective radius of droplets in warm stratocumulus clouds, J. Atmos. Sci., 51, 1823–1842, 1994. 15506, 15520, 15521

Miles, N. L., Verlinde, J., and Clothiaux, E. E.: Cloud droplet size distributions in low-level stratiform clouds, J. Atmos. Sci., 57, 295–311, 2000. 15506, 15521

Mlawer, E. J., Taubman, S. J., Brown, P. D., Iacono, M. J., and Clough, S. A.: Radiative transfer for inhomogeneous atmospheres: RRTM, a validated correlated-k model for the longwave, J. Geophys. Res., 102, 16663–16682, 1997. 15510

Moeng, C.-H., Dudhia, J., Klemp, J. B., and Sullivan, P. P.: Examining two-way grid nesting for large eddy simulation of the PBL using the WRF model, Mon. Weather Rev., 135, 2295–2311, doi:10.1175/MWR3406.1, 2007. 15508

Petters, M. D. and Kreidenweis, S. M.: A single parameter representation of hygroscopic growth and cloud condensation nucleus activity, Atmos. Chem. Phys., 7, 1961–1971, doi:10.5194/acp-7-1961-2007, 2007. 15509

Pincus, R. and Baker, M. B.: Effect of precipitation on the albedo susceptibility of marine boundary layer clouds, Nature, 372, 250–252, 1994. 15507

Pruppacher, H. R. and Klett, J. D.: Microphysics of Clouds and Precipitation, Kluwer Academic Publishers, Boston, USA, 954 pp., 1997. 15505, 15509, 15535

Randall, D. A., Coakley Jr., J. A., Fairall, C. W., Kropfli, R. A., and Lenschow, D. H.: Outlook for research on subtropical marine stratiform clouds, B. Am. Meteorol. Soc., 65, 1290–1301, 1984. 15499

Rasmussen, R. M., Geresdi, I., Thompson, G., Manning, K., and Karplus, E.: Freezing drizzle formation in stably stratified layer clouds: The role of radiative cooling of cloud droplets, cloud condensation nuclei, and ice initiation, J. Atmos. Sci., 59, 837–860, 2002. 15508

Reisin, T., Levin, Z., and Tzivion, S.: Rain production in convective clouds as simulated in an axisymmetric model with detailed microphysics. Part I: description of the model, J. Atmos. Sci., 53, 497–519, 1996. 15508

Rotstayn, L. D. and Liu, Y.: Sensitivity of the first indirect aerosol effect to an increase of cloud droplet spectral dispersion with droplet number concentration, J. Climate, 16, 3476–3481,

ACPD
11, 15497–15550, 2011

2003. 15506, 15535

Rotstayn, L. D. and Liu, Y.: Cloud droplet spectral dispersion and the indirect aerosol effect: Comparison of two treatments in a GCM, Geophys. Res. Lett., 36, L10801, doi:10.1029/2009GL038216, 2009. 15506

Sandu, I., Brenguier, J., Geoffroy, O., Thouron, O., and Masson, V.: Aerosol impacts on the diurnal cycle of marine stratocumulus, J. Atmos. Sci., 65, 2705–2718, 2008. 15500, 15502, 15534

Sandu, I., Brenguier, J., Thouron, O., and Stevens, B.: How important is the vertical structure for the representation of aerosol impacts on the diurnal cycle of marine stratocumulus?, Atmos. Chem. Phys., 9, 4039–4052, doi:10.5194/acp-9-4039-2009, 2009. 15499

Savic-Jovcic, V. and Stevens, B.: The structure and mesoscale organization of precipitating stratocumulus, J. Atmos. Sci., 65, 1587–1605, 2008. 15500

Seinfeld, J. H. and Pandis, S. N.: Atmospheric Chemistry and Physics, John Wiley and Sons, Inc., Hoboken, NJ, USA, 2 edn., 2006. 15514

Shao, H. and Liu, G.: A critical examination of the observed first aerosol indirect effect, J. Atmos. Sci., 66, 1018–1032, 2009. 15505, 15535

Stevens, B.: Atmospheric moist convection, Annu. Rev. Earth Pl. Sc., 33, 605–643, doi:10.1146/annurev.earth.33.092203.122658, 2005. 15499

Stevens, B.: Bulk boundary-layer concepts for simplified models of tropical dynamics, Theor. Comp. Fluid Dyn., 20, 279–304, doi:10.1007/s00162-006-0032-z, 2006. 15499

Stevens, B. and Brenguier, J.-L.: Cloud controlling factors: low clouds, in: Clouds in the perturbed climate system: their relationship to energy balance, atmospheric dynamics, and precipitation, edited by: Heintzenberg, J. and Charlson, R. J., 173–196, MIT Press, 2009. 15499, 15500

Stevens, B. and Feingold, G.: Untangling aerosol effects on clouds and precipitation in a buffered system, Nature, 461, 607–613, doi:10.1038/nature08281, 2009. 15499

Stevens, B., Cotton, W. R., Feingold, G., and Moeng, C.-H.: Large-eddy simulations of strongly precipitating, shallow, stratocumulus-topped boundary layers, J. Atmos. Sci., 55, 3616–3638, 1998. 15500, 15501, 15513

Stevens, B., Lenschow, D. H., Faloona, I., Moeng, C.-H., Lilly, D. K., Blomquist, B., Vali, G., Bandy, A., Campos, T., Gerber, H., Haimov, S., Morley, B., and Thornton, D.: On entrainment rates in nocturnal marine stratocumulus, Q. J. Roy. Meteorol. Soc., 129, 3469–3493, doi:10.1256/qj.02.202, 2003. 15500

ACPD

11, 15497–15550, 2011

Aerosol-cloud-precipitation interactions in MSc

Y.-C. Chen et al.

Stevens, B., Moeng, C.-H., Ackerman, A. S., Bretherton, C. S., Chlond, A., De Roode, S., Edwards, J., Golaz, J., Jiang, H., Khairoutdinov, M., Kirkpatrick, M. P., Lewellen, D. C., Lock, A., Muller, F., Stevens, D. E., Whelan, E., and Zhu, P.: Evaluation of large-eddy simulations via observations of nocturnal marine stratocumulus, Mon. Weather Rev., 133, 1443–1462, 2005. 15500
Stevens, D. E. and Bretherton, C. S.: Effects of resolution on the simulation of stratocumulus entrainment, Q. J. Roy. Meteorol. Soc., 125, 425–439, 1999. 15500
Turton, J. and Nicholls, S.: A study of the diurnal variation of stratocumulus using a multiple mixed-layer model, Q. J. Roy. Meteorol. Soc., 113, 969–1011, 1987. 15499
Twomey, S.: The nuclei of natural cloud formation Part 2: The supersaturation in natural clouds and the variation of cloud droplet concentration, Pure Appl. Geophys., 43, 243–249, 1959. 15505
Twomey, S.: The influence of pollution on the shortwave albedo of clouds, J. Atmos. Sci., 34, 1149–1152, 1977. 15500
Tzivion, S., Feingold, G., and Levin, Z.: An efficient numerical solution to the stochastic collection equation, J. Atmos. Sci., 44, 3139–3149, 1987. 15508
Tzivion, S., Feingold, G., and Levin, Z.: The evolution of raindrop spectra. Part II: collisional collection/breakup and evaporation in a rainshaft, J. Atmos. Sci., 46, 3312–3327, 1989. 15508
Uchida, J., Bretherton, C. S., and Blossey, P. N.: The sensitivity of stratocumulus-capped mixed layers to cloud droplet concentration: do LES and mixed-layer models agree?, Atmos. Chem. Phys., 10, 4097–4109, doi:10.5194/acp-10-4097-2010, 2010. 15499, 15500
Wang, H. and Feingold, G.: Modeling mesoscale cellular structures and drizzle in marine stratocumulus. Part I: Impact of drizzle on the formation and evolution of open cells, J. Atmos. Sci., 66, 3237–3256, 2009a. 15500, 15508
Wang, H. and Feingold, G.: Modeling mesoscale cellular structures and drizzle in marine stratocumulus. Part II: The microphysics and dynamics of the boundary region between open and closed cells, J. Atmos. Sci., 66, 3257–3275, 2009b. 15500, 15508
Wang, H., Skamarock, W. C., and Feingold, G.: Evaluation of scalar advection schemes in the advanced research WRF model using large-eddy simulations of aerosol-cloud interactions, Mon. Weather Rev., 137, 2547–2558, doi:10.1175/2009MWR2820.1, 2009. 15508, 15510
Wang, H., Feingold, G., Wood, R., and Kazil, J.: Modeling microphysical and meteorological controls on precipitation and cloud cellular structures in Southeast Pacific stratocumulus, Atmos. Chem. Phys., 10, 6347–6362, doi:10.5194/acp-10-6347-2010, 2010. 15500, 15534

ACPD
11, 15497–15550, 2011
Aerosol-cloud-precipitation interactions in MSc
Y.-C. Chen et al.

Wang, S., Wang, Q., and Feingold, G.: Turbulence, condensation, and liquid water transport in numerically simulated nonprecipitating stratocumulus clouds, J. Atmos. Sci., 60, 262–278, 2003. 15500, 15501

Warren, S. G., Hahn, C. J., London, J., Chervine, R. M., and Jenne, R. L.: Global distribution of total cloud cover and cloud type amounts over the ocean, NCAR/TN-317 STR, NCAR Tech. Note., 41 pp., 1988. 15499

Wood, R.: Cancellation of aerosol indirect effects in marine stratocumulus through cloud thinning, J. Atmos. Sci., 64, 2657–2669, doi:10.1175/JAS3942.1, 2007. 15499, 15501, 15507, 15523, 15524, 15534, 15535

Wood, R., Irons, S., and Jonas, P. R.: How important is the spectral ripening effect in stratiform boundary layer clouds? Studies using simple trajectory analysis, J. Atmos. Sci., 59, 2681–2693, 2002. 15506

Xue, H. and Feingold, G.: Large-eddy simulations of trade wind cumuli: Investigation of aerosol indirect effects, J. Atmos. Sci., 63, 1605–1622, 2006. 15501, 15502

Xue, L., Teller, A., Rasmussen, R. M., Geresdi, I., and Pan, Z.: Effects of aerosol solubility and regeneration on warm-phase orographic clouds and precipitation simulated by a detailed bin microphysical scheme, J. Atmos. Sci., 67, 3336–3354, doi:10.1175/2010JAS3511.1, 2010. 15508

Yamaguchi, T. and Randall, D. A.: Large-eddy simulation of evaporatively driven entrainment in cloud-topped mixed layers, J. Atmos. Sci., 65, 1481–1504, 2008. 15500

ACPD
11, 15497–15550, 2011

Aerosol-cloud-precipitation interactions in MSc

Y.-C. Chen et al.

Table 1. Studies of aerosol-cloud interactions in MSc.

	Nighttime			Daytime		Diurnal Mean*
	Non-drizzling	Drizzling		Non-drizzling	Drizzling	
		Light	Moderate/ Heavy		Light	Moderate/ Heavy
Ackerman et al. (2004)		$N_\mathrm{a}\uparrow \Longrightarrow \mathrm{LWP}\downarrow$ $q_\mathrm{ft}\downarrow \Longrightarrow \mathrm{LWP}\downarrow$	$N_\mathrm{a}\uparrow \Longrightarrow P\downarrow \Longrightarrow \mathrm{LWP}\uparrow$			
Lu and Seinfeld (2005)		$N_\mathrm{a}\uparrow \Longrightarrow \mathrm{LWP}\downarrow$ $\mathrm{SST}\uparrow \Longrightarrow \mathrm{LWP}\downarrow$ $D\uparrow \Longrightarrow \mathrm{LWP}\downarrow$	$N_\mathrm{a}\uparrow \Longrightarrow P\downarrow \Longrightarrow \mathrm{LWP}\uparrow$	$N_\mathrm{a}\uparrow \Longrightarrow \mathrm{LWP}\downarrow$		
Wood (2007)						$N_\mathrm{a}\uparrow \Longrightarrow H\downarrow$ or $\uparrow$
Sandu et al. (2008)			$N_\mathrm{a}\uparrow \Longrightarrow P\downarrow \Longrightarrow \mathrm{LWP}\uparrow$ $D\uparrow \Longrightarrow \mathrm{LWP}\downarrow$ $q_\mathrm{ft}\downarrow \Longrightarrow \mathrm{LWP}\downarrow$		$N_\mathrm{a}\uparrow \Longrightarrow \mathrm{LWP}\downarrow$ $D\uparrow \Longrightarrow \mathrm{LWP}\downarrow$ $q_\mathrm{ft}\downarrow \Longrightarrow \mathrm{LWP}\downarrow$	
Hill et al. (2008, 2009)	$N_\mathrm{a}\uparrow \Longrightarrow \mathrm{LWP}\downarrow$			$N_\mathrm{a}\uparrow \Longrightarrow \mathrm{LWP}\downarrow$		
Wang et al. (2010)			$N_\mathrm{a}\uparrow \Longrightarrow P\downarrow \Longrightarrow \mathrm{LWP}\uparrow$		$N_\mathrm{a}\uparrow \Longrightarrow \mathrm{LWP}\downarrow$	
Caldwell and Bretherton (2009a)		$N_\mathrm{a}\uparrow \Longrightarrow \mathrm{LWP}\downarrow$ $\mathrm{SST}\uparrow \Longrightarrow \mathrm{LWP}\uparrow$				
Summary	$N_\mathrm{a}\uparrow \Longrightarrow \mathrm{LWP}\downarrow$	$N_\mathrm{a}\uparrow \Longrightarrow \mathrm{LWP}\downarrow$ $\mathrm{SST}\uparrow \Longrightarrow \mathrm{LWP}\downarrow$ or $\uparrow$ $D\uparrow \Longrightarrow \mathrm{LWP}\downarrow$ $q_\mathrm{ft}\downarrow \Longrightarrow \mathrm{LWP}\downarrow$	$N_\mathrm{a}\uparrow \Longrightarrow P\downarrow \Longrightarrow \mathrm{LWP}\uparrow$ $D\uparrow \Longrightarrow \mathrm{LWP}\downarrow$ $q_\mathrm{ft}\downarrow \Longrightarrow \mathrm{LWP}\downarrow$	$N_\mathrm{a}\uparrow \Longrightarrow \mathrm{LWP}\downarrow$	$N_\mathrm{a}\uparrow \Longrightarrow \mathrm{LWP}\downarrow$ $D\uparrow \Longrightarrow \mathrm{LWP}\downarrow$ $q_\mathrm{ft}\downarrow \Longrightarrow \mathrm{LWP}\downarrow$	$N_\mathrm{a}\uparrow \Longrightarrow H\downarrow$ or $\uparrow$

P is surface precipitation, H is cloud thickness, D is large-scale divergence rate, and q_ft is free tropospheric humidity. Light drizzle is defined as surface precipitation rate <0.1 mm day^{-1}, and moderate/heavy drizzle >0.1 mm day^{-1}.

* Wood (2007) uses the downwelling shortwave radiation close to the annual diurnal mean value over the subtropical regions.

ACPD
11, 15497–15550, 2011

Table 2. Sign and magnitude of each term in Eq. (3) from previous studies.

	$\frac{\Delta(\ln N_d)}{\Delta(\ln N_a)}$	$\frac{\Delta(\ln k)}{\Delta(\ln N_d^*)}$	$\frac{\Delta(\ln H)}{\Delta(\ln N_d^*)}$	$\frac{\Delta(\ln \tau)}{\Delta(\ln N_a)}$
Measurement	0.6–0.9[a]	−0.2[c]		
	0.25–0.85[b]	−0.14[d]		
LES	0.91[e] (constant LWP)	~0.03 (light drizzle)[f]	$\frac{\partial(\ln LWP)}{\partial(\ln N_a)}^{e} = -0.1$ (clean)	0.22 (clean)[e]
		~0.2 (heavy drizzle)[f]	−0.03 (polluted)	0.28 (polluted)[e]
Other			cloud base >400 m: thinning[g] cloud base <400 m: thickening[g]	0.28[h]

[*] Note N_d is applied rather than N_a.
[a] Pruppacher and Klett (1997)
[b] Shao and Liu (2009), based on in-situ measurements.
[c] Rotstayn and Liu (2003), including measurements from FIRE, SOCEX, ACE1, ASTEX, SCMS, INDOEX, MAST, etc.
[d] Ackerman et al. (2000)
[e] Lu and Seinfeld (2005): LES based on sounding profiles from FIRE and ASTEX. Note LWP is applied rather than *H*.
[f] Lu and Seinfeld (2006): LES based on sounding profiles from FIRE and ASTEX.
[g] Wood (2007): obtained by MLM and analytical formulations.
[h] Hill et al. (2009) Table 4.

ACPD
11, 15497–15550, 2011

Table 3. Summary of simulated cases.

	N_a (cm^{-3})	Domain (km^2)	SST (K)	q_{ft} ($g\,kg^{-1}$)	D (s^{-1})	U,V (ms^{-1})
Control	100, 200, 1000	1×1, 2.5×2.5	288	6.1	5.5	x: −1, y:6
SST290, SST292	100, 1000	1×1	290, 292			
QFT3, QFT1	100, 1000	1×1		3.1, 1.1		
DIV3, DIV8	100, 1000	1×1			3.0, 8.0	
WIND	100, 1000	1×1				x: −4, y:10

ACPD
11, 15497–15550, 2011

Table 4. Estimation of aerosol-induced effects on MSc cloud properties from the LES model and of cloud susceptibility from Eq. (3) for specific sensitivity simulations under nighttime (4–7 h) and daytime (12–15 h) conditions; aerosol number concentrations considered are 100, 200, 500, and 1000 cm^{-3}.

		$\frac{\Delta(\ln N_d)}{\Delta(\ln N_a)}$		$\frac{\Delta(\ln k)}{\Delta(\ln N_a)}$		$\frac{\Delta(\ln H)}{\Delta(\ln N_a)}$		$\frac{\Delta(\ln \tau)}{\Delta(\ln N_a)}$		$\frac{\Delta(\ln \tau)}{\Delta(\ln N_a)}$ (Eq. 3)	
		Night	Day	Night	Day	Night	Day	Night	Day	Night	Day
Control	Mean	1.077	1.158	0.072	0.094	−0.014	−0.126	0.350	0.261	0.360	0.207
	Stdev	0.049	0.029	0.016	0.030	0.010	0.034	0.035	0.104		
SST290	Mean	1.000	0.805	0.036	0.050	−0.038	−0.346	0.280	−0.358	0.282	−0.292
	Stdev	0.023	0.086	0.010	0.023	0.007	0.160	0.018	0.370		
QFT3	Mean	1.000	1.037	0.026	0.070	−0.026	−0.120	0.291	0.165	0.299	0.169
	Stdev	0.010	0.025	0.006	0.036	0.016	0.011	0.026	0.039		
DIV3	Mean	1.245	1.370	0.150	0.082	0.014	−0.005	0.528	0.625	0.488	0.476
	Stdev	0.128	0.070	0.047	0.018	0.013	0.050	0.120	0.154		

Discussion Paper | Discussion Paper | Discussion Paper | Discussion Paper |
ACPD
11, 15497–15550, 2011
Aerosol-cloud-precipitation interactions in MSc
Y.-C. Chen et al.

Table 5. Values of environmental variables.

Variable	Values
SST (K)	288, 290, 292
q_{ft} ($g\,kg^{-1}$)	1.1, 3.1, 6.1
D ($10^{-6}\,s^{-1}$)	3.0, 5.5, 8.0

ACPD
11, 15497–15550, 2011

Aerosol-cloud-precipitation interactions in MSc

Y.-C. Chen et al.

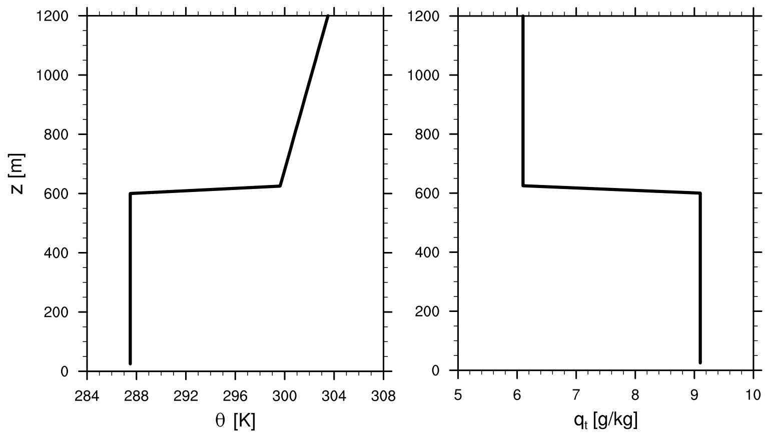

Fig. 1. Initial sounding profile (potential temperature θ and total water mixing ratio q_t) for the MSc of Control case.

ACPD
11, 15497–15550, 2011

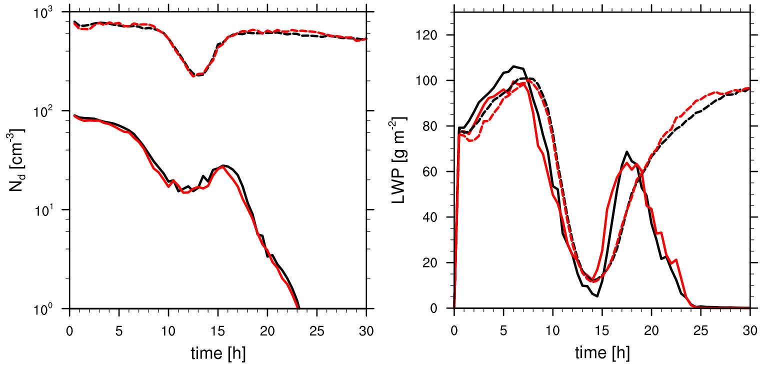

Fig. 2. Time evolution of N_d and LWP under different domain size: $2.5 \times 2.5\,\text{km}^2$ (black) and $1 \times 1\,\text{km}^2$ (red); under different N_a: clean (solid line) and polluted (dashed line) cloud.

ACPD
11, 15497–15550, 2011

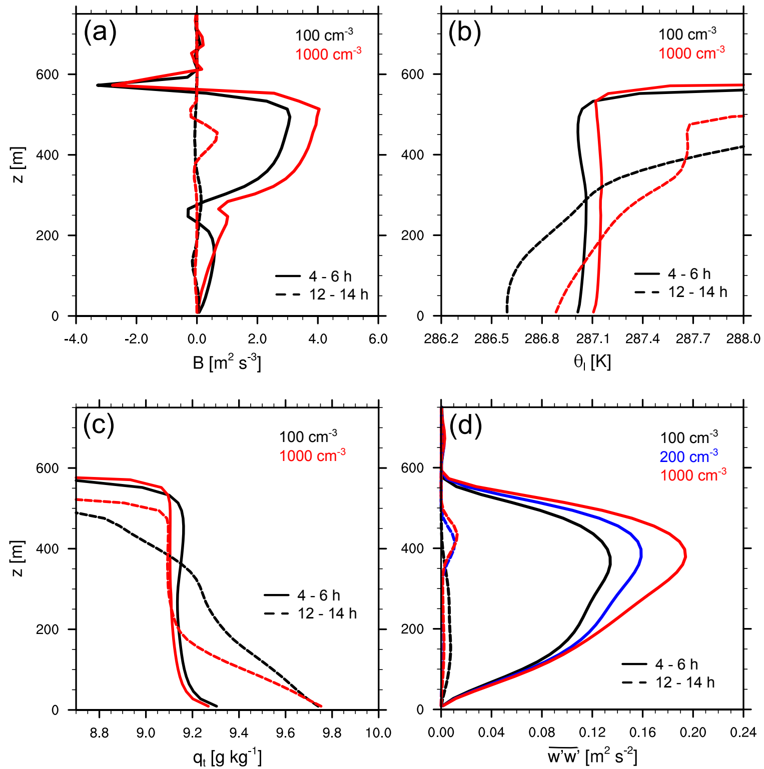

Fig. 3. Vertical profile averaged over 4–6 h (solid line) and 12–14 h (dashed line) of **(a)** mean buoyancy flux, $B = \frac{g}{\theta_v}\overline{w'\theta_v{}'}$, where θ_v is virtual potential temperature, **(b)** mean liquid water potential temperature θ_l, **(c)** mean total water mixing ratio q_t, and **(d)** mean vertical velocity variance of clean (black), semi-polluted (blue), and polluted (red) cloud.

ACPD
11, 15497–15550, 2011

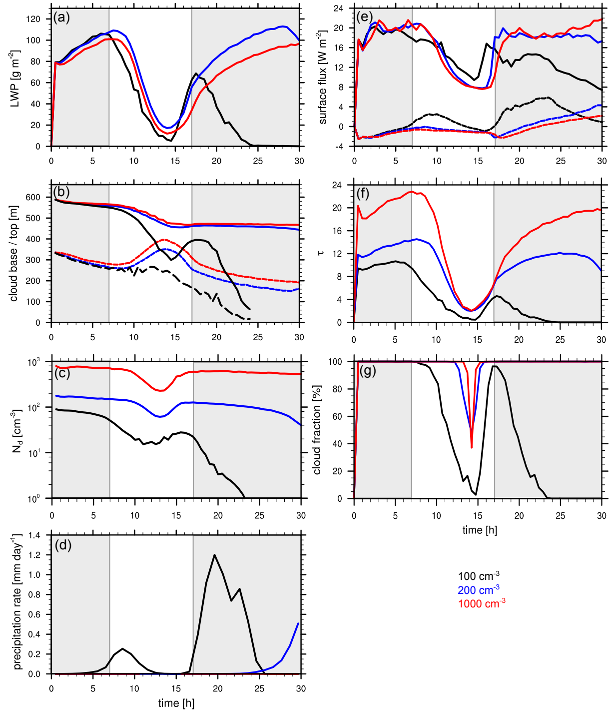

Fig. 4. Cloud properties of Control case with a 2.5×2.5 km^2 horizontal domain for clean (black), semi-polluted (blue), and polluted (red) clouds. Figures are the time evolution of: **(a)** average LWP; **(b)** average cloud top (solid line) and cloud base (dashed line) height, where the cloudy grid is defined as grid with cloud water mixing ratio >0.01 g kg^{-1}; **(c)** cloud droplet number concentration N_d, averaged over the cloudy grid; **(d)** surface precipitation rate, hourly averaged; **(e)** domain average surface latent (solid line) and sensible (dashed line) heat flux; **(f)** average cloud optical depth; **(g)** cloud fraction, defined by cloud optical depth >2. Gray regions are for the nighttime conditions (0–7 h and 17–30 h), while write regions are for the daytime conditions (7–17 h).

ACPD
11, 15497–15550, 2011

Title Page
Abstract | Introduction
Conclusions | References
Tables | Figures
◂| |▸
◂ ▸
Back | Close
Full Screen / Esc
Printer-friendly Version
Interactive Discussion

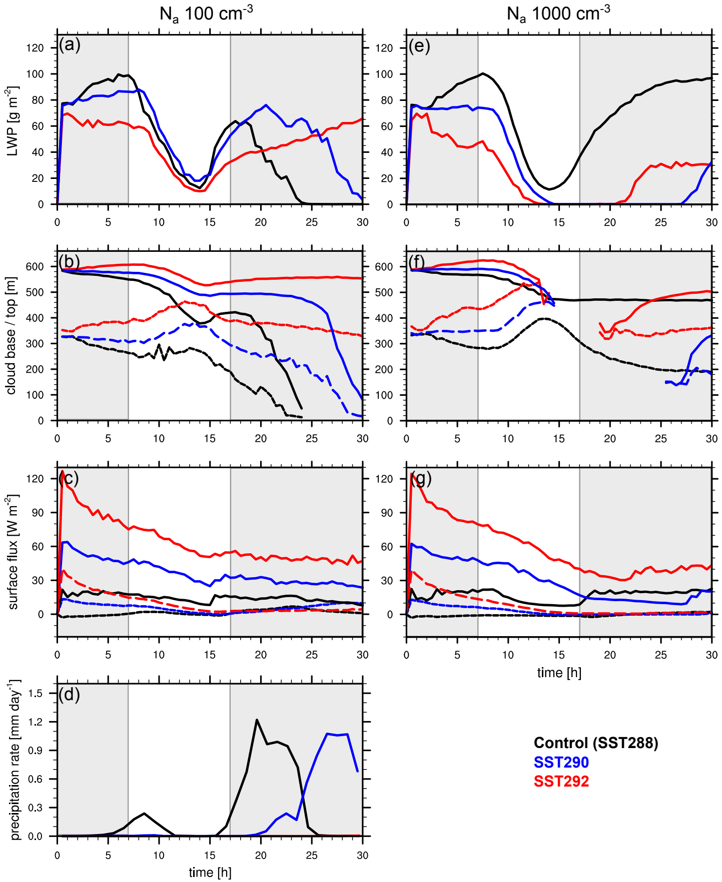

Fig. 5. Time evolution of $1 \times 1\,\mathrm{km}^2$ clean ($N_a = 100\,\mathrm{cm}^{-3}$, left column) and polluted ($N_a = 1000\,\mathrm{cm}^{-3}$, right column) cloud for Control (black), SST290 (blue) and SST292 (red) case: **(a)** and **(e)** average LWP; **(b)** and **(f)** average cloud top/base height; **(c)** and **(g)** domain average surface latent (solid line) and sensible (dashed line) heat flux; **(d)** surface precipitation rate, hourly averaged.

ACPD
11, 15497–15550, 2011

Aerosol-cloud-precipitation interactions in MSc

Y.-C. Chen et al.

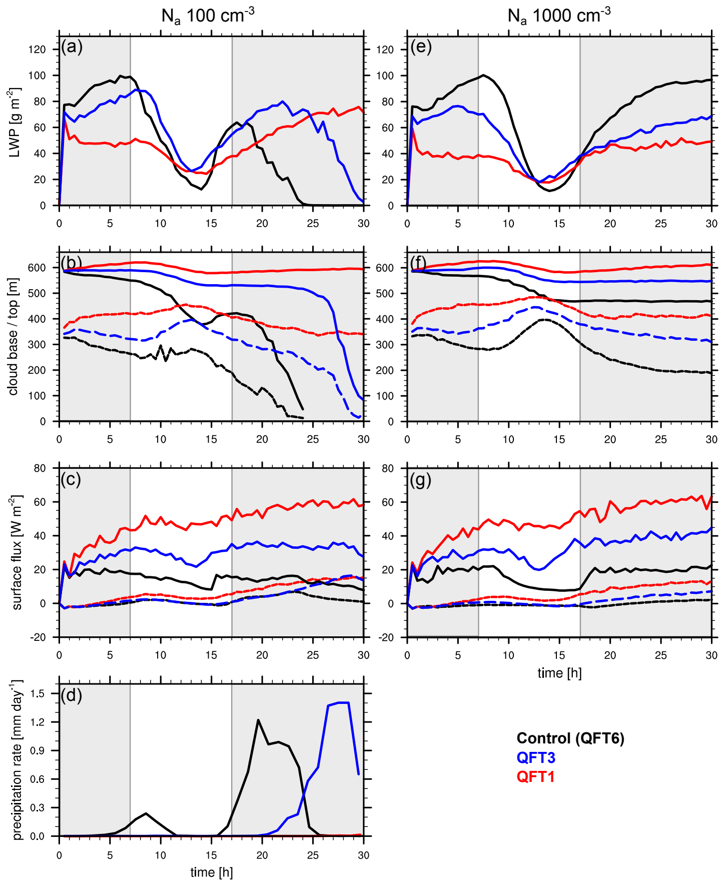

Fig. 6. The same as Fig. 5, except for Control (black), QFT3 (blue) and QFT1 (red) case.

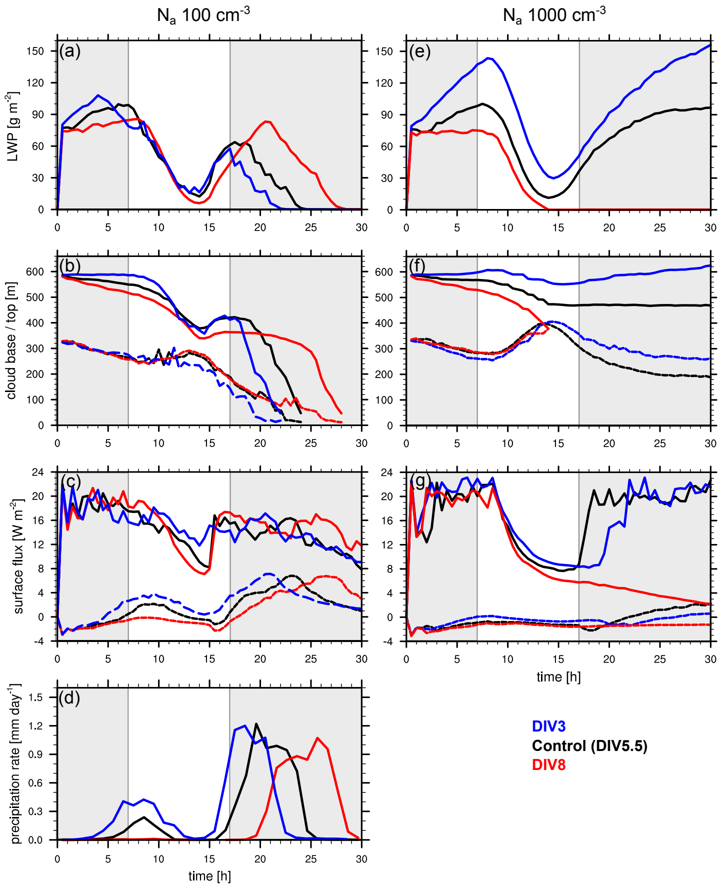

Fig. 7. The same as Fig. 5, except for Control (black), DIV3 (blue) and DIV8 (red) case.

ACPD
11, 15497–15550, 2011

Aerosol-cloud-precipitation interactions in MSc

Y.-C. Chen et al.

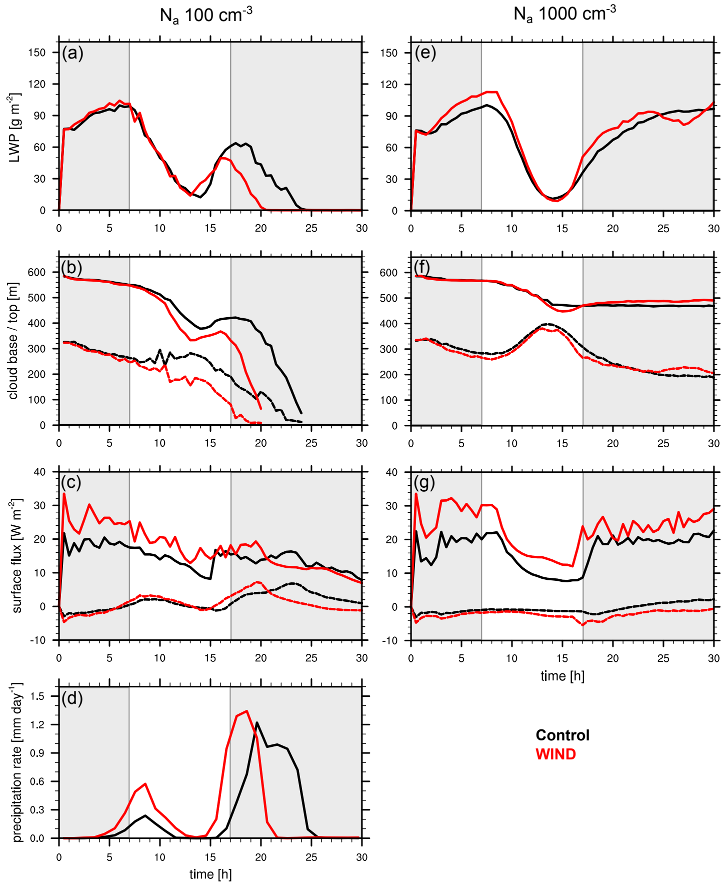

Fig. 8. The same as Fig. 5, except for Control (black) and WIND (red) case.

ACPD
11, 15497–15550, 2011

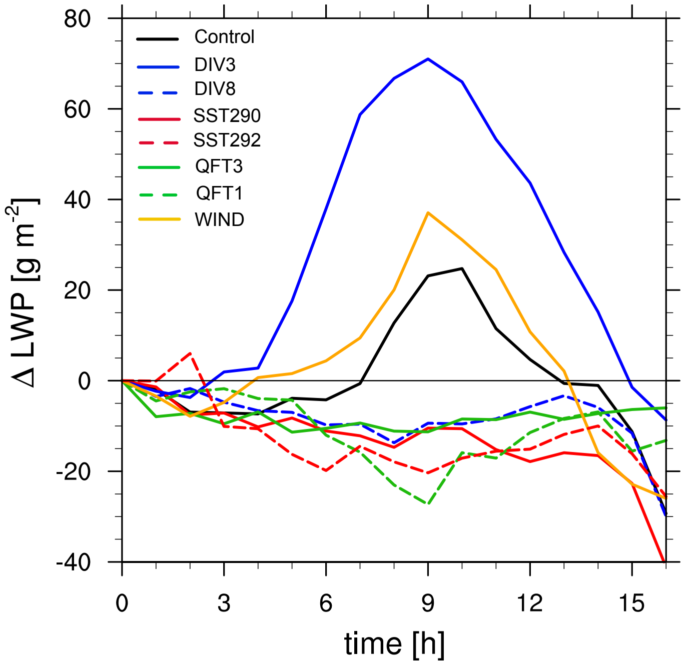

Fig. 9. Time evolution of LWP difference between polluted and clean cloud for Control (black), SST290 (red solid), SST292 (red dashed), QFT3 (green solid), QFT1 (green dashed), DIV3 (blue solid), DIV8 (blue dashes), and WIND (orange) case.

ACPD
11, 15497–15550, 2011

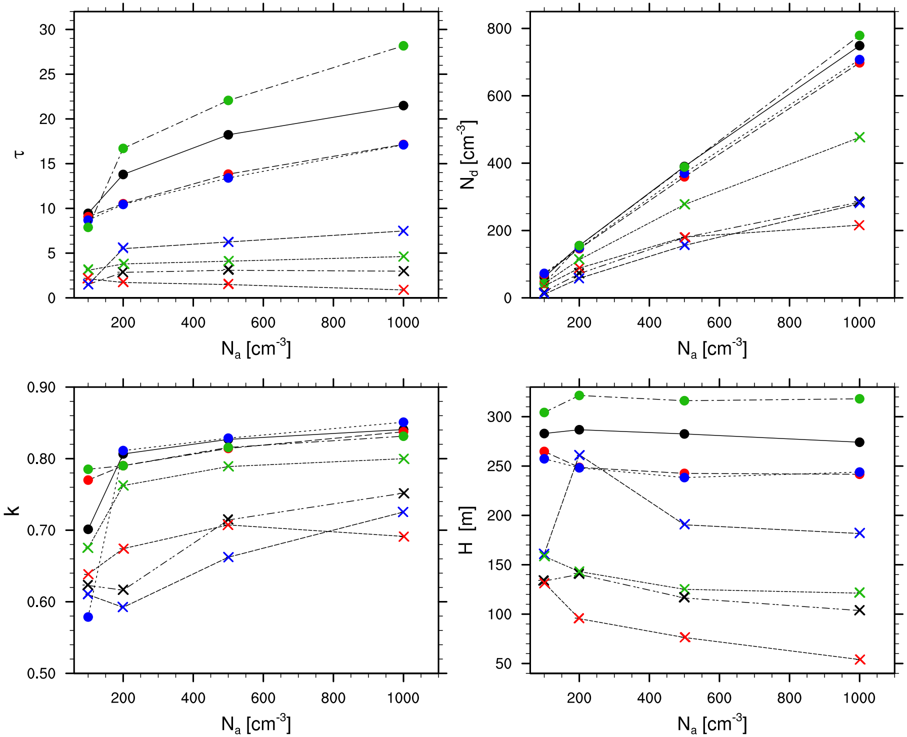

Fig. 10. Averaged optical depth (τ), cloud droplet number concentration (N_d), dispersion coefficient (k) and cloud thickness (H) as a function of aerosol number concentration N_a. Values are averaged horizontally and vertically between cloud top and base for Control (black), SST290 (red), QFT3 (blue), and DIV3 (green) cases during nighttime (averaged over 4–7 h, filled circle) and daytime (average over 12–15 h, cross).

ACPD
11, 15497–15550, 2011

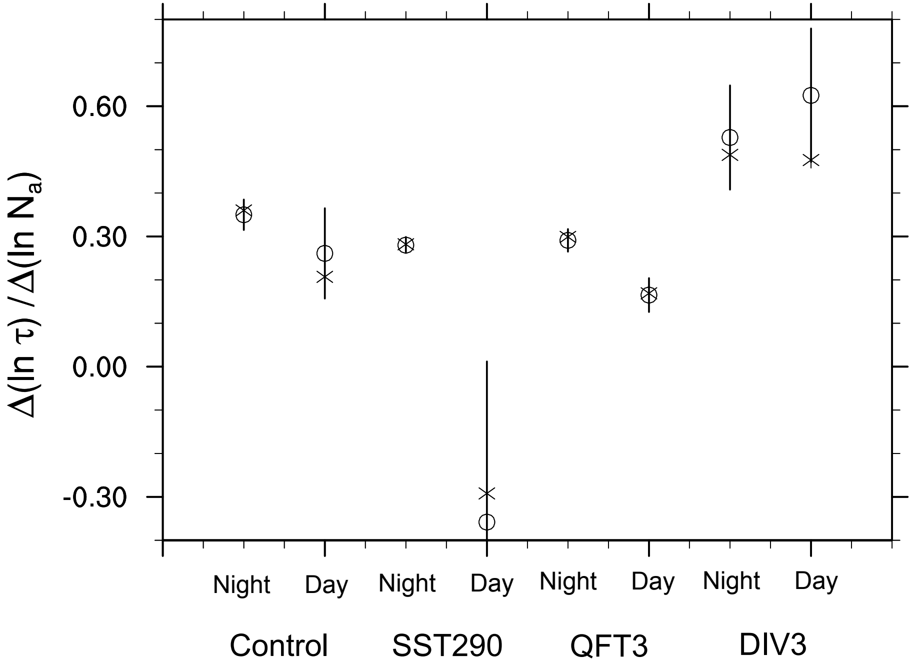

Fig. 11. Averaged $\Delta(\ln\tau)/\Delta(\ln N_a)$ from the LES model (unfilled circle) and Eq. (3) (asterisk) for specific sensitivity simulations under nighttime (4–7 h) and daytime (12–15 h), as shown in last two columns of Table 4. The error bar (standard deviation) is computed from LES experiments.

ACPD
11, 15497–15550, 2011

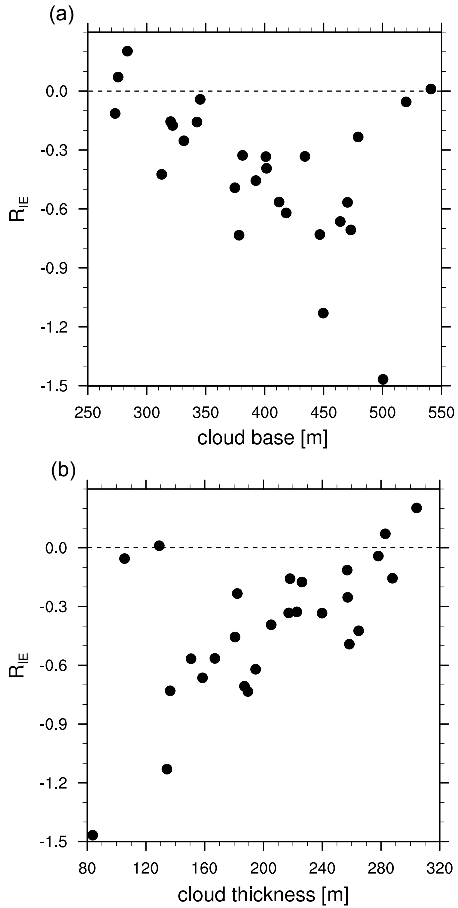

Fig. 12. The mean ratio of second to first indirect effect (R_{IE}) for N_a from 100 to 200 cm^{-3} as a function of **(a)** cloud base height, and **(b)** cloud thickness. The data points are averaged over 4–7 h.

ACPD

11, 15497–15550, 2011

Aerosol-cloud-precipitation interactions in MSc

Y.-C. Chen et al.